

INVESTIGATION OF THE PHASE TRANSITIONS
IN THE ALKALI METAL NITRITES USING
RAMAN SPECTROSCOPY

CENTRE FOR NEWFOUNDLAND STUDIES

**TOTAL OF 10 PAGES ONLY
MAY BE XEROXED**

(Without Author's Permission)

ROBIN V. WALTERS





National Library
of Canada

Bibliothèque nationale
du Canada

Canadian Theses Service Service des thèses canadiennes

Ottawa, Canada
K1A 0N4

The author has granted an irrevocable non-exclusive licence allowing the National Library of Canada to reproduce, loan, distribute or sell copies of his/her thesis by any means and in any form or format, making this thesis available to interested persons.

The author retains ownership of the copyright in his/her thesis. Neither the thesis nor substantial extracts from it may be printed or otherwise reproduced without his/her permission.

L'auteur a accordé une licence irrévocable et non exclusive permettant à la Bibliothèque nationale du Canada de reproduire, prêter, distribuer ou vendre des copies de sa thèse de quelque manière et sous quelque forme que ce soit pour mettre des exemplaires de cette thèse à la disposition des personnes intéressées.

L'auteur conserve la propriété du droit d'auteur qui protège sa thèse. Ni la thèse ni des extraits substantiels de celle-ci ne doivent être imprimés ou autrement reproduits sans son autorisation.

ISBN 0-315-54987-4

**Investigation of the Phase Transitions in the Alkali Metal Nitrites
using Raman Spectroscopy**

by



Robin V. Walters

A thesis submitted in partial fulfillment of the requirements for the degree of Masters of Science.

**Department of Chemistry
Memorial University of Newfoundland**

July, 1989

St. John's

Newfoundland

Table of Contents

	Page
Dedication	ii
Acknowledgement	iii
List of Figures	iv
List of Tables	ix
Abstract	1
Introduction	2
Theory	9
Experimental	20
Results and Discussion	28
Conclusion	162
References	163
Appendix 1	168

DEDICATION

To my parents for their never-ending love and support.

ACKNOWLEDGEMENT

I would like to acknowledge with much gratitude Dr. M.H. Brooker, my project supervisor, for his assistance and guidance during the work and for his expertise in helping to interpret the results. I also thank the following people for their assistance; Bernard Rice for his writing of the computer programs used, Teresa Barker for typing my thesis, John Kane for preparing some of the figures, and the various workers in our group for their support and assistance.

List of Figures

	Page
Figure 1. Motions of a one-dimensional crystal.	15
Figure 2. Comparison of vibrational spectra for ordered and disordered solids.	17
Figure 3a. Glass evaporating cryostat.	24
Figure 3b. Coderg circulating N ₂ cryostat.	25
Figure 4. Oven for measurement of Raman spectra at high temperature.	26
Figure 5. Schematic representation of Laser Raman apparatus used to measure spectra.	27
Figure 6. Raman spectrum of LiNO ₂ recorded at 77 K using the blue 4880 Å line. $\nu_{\text{initial}} = 30 \text{ cm}^{-1}$	30
Figure 7. Raman spectrum of LiNO ₂ sealed under NO(g) recorded at room temperature using the blue 4880 Å line. $\nu_{\text{initial}} = 60 \text{ cm}^{-1}$	32
Figure 8. Raman spectrum of LiNO ₂ sealed under NO(g) recorded at 471 K using the blue 4880 Å line. $\nu_{\text{initial}} = 60 \text{ cm}^{-1}$. There is no evidence for a high temperature phase. Peaks in the low frequency region are thermally expanded lattice modes of the low temperature phase.	34
Figure 9. Intensity, $I(\omega)$, Raman spectra of LiNO ₂ melt under NO(g) recorded at 505 K using the blue 4880 Å line. $\nu_{\text{initial}} = 60 \text{ cm}^{-1}$	36
Figure 10. Reduced, $R(\omega)$, Raman spectra of LiNO ₂ melt under NO(g) recorded at 505 K using the blue 4880 Å line. $\nu_{\text{initial}} = 60 \text{ cm}^{-1}$	38
Figure 11. Temperature dependence of ν_1 and ν_2 frequencies and halfwidths for LiNO ₂	41
Figure 12. Unit-cell of NaNO ₂ , ferroelectric, C _{2v} ²⁰ point group symmetry. Dashed circles represent the paraelectric phase, D _{2h} ²⁵ , where nitrite is on two distinct sites.	45

- Figure 13. Raman spectrum of NaNO_2 powder which was never melted, recorded at 77 K using the blue 4880 Å line. $\nu_{\text{initial}} = 31 \text{ cm}^{-1}$. The NaNO_2 , III, is in an ordered ferroelectric phase. 48
- Figure 14. Raman spectrum of a NaNO_2 single crystal recorded at 298 K using the blue 4880 Å line. $\nu_{\text{initial}} = 20 \text{ cm}^{-1}$. This is the "regular" orientation with ν_3 at 1228 cm^{-1} . The B_1 (TO) modes are allowed but there is some spill-over of the A_1 (TO) modes (827 and 1324 cm^{-1}) and the A_2 mode (119 cm^{-1}). The phase is ferroelectric. 50
- Figure 15. Intensity, $I(\omega)$, Raman spectra of NaNO_2 melt recorded at 573 K using the green 5145 Å line. $\nu_{\text{initial}} = 44 \text{ cm}^{-1}$ 52
- Figure 16. Reduced, $R(\omega)$, Raman spectra of NaNO_2 melt recorded at 573 K using the green 5145 Å line. $\nu_{\text{initial}} = 44 \text{ cm}^{-1}$ 54
- Figure 17. Raman spectrum of paraelectric, disordered NaNO_2 I recorded at 539 K using the blue 4880 Å line. $\nu_{\text{initial}} = 50 \text{ cm}^{-1}$ 56
- Figure 18. Raman spectrum of a NaNO_2 oriented single crystal recorded at 77 K using the blue 4880 Å line. $\nu_{\text{initial}} = 20 \text{ cm}^{-1}$. The ν_3 LO mode is positioned at 1358.5 cm^{-1} , shifted $\sim 128 \text{ cm}^{-1}$ from its "regular" frequency. The crystal orientation is $y(xz)x$ where x and y are 110 planes. 58
- Figure 19. Raman spectrum of a NaNO_2 oriented single crystal recorded at 298 K using the blue 4880 Å line. $\nu_{\text{initial}} = 30 \text{ cm}^{-1}$. The ν_3 LO mode has shifted $\sim 128 \text{ cm}^{-1}$ from its "regular" frequency. Also, the ν_3 mode is approximately two times as intense as the ν_1 mode. Crystal orientation is $y(xz)x$ where x and y are 110 planes. 60
- Figure 20. Intensity, $I(\omega)$, Raman spectra of the ν_1, ν_3 region of NaNO_2 oriented single crystal as it went through the order-disorder phase transition. Spectra were recorded using the blue 4880 angstrom line at: A) 298 K; B) 383 K; C) 413 K; D) 434 K; and E) 458 K. $\nu_{\text{initial}} = 30 \text{ cm}^{-1}$. ν_3 shifted $\sim 105 \text{ cm}^{-1}$. Crystal orientation is $y(xz)x$ where x and y are 110 planes. 62
- Figure 21. Raman spectrum of NaNO_2 oriented single crystal at 434 K recorded using the blue 4880 Å line. $\nu_{\text{initial}} = 30 \text{ cm}^{-1}$. The

ν_3 mode appears at its "regular" and "oriented" frequencies as it neared the 436 K phase transition. Crystal orientation is $y(xz)x$ where x and y are 110 planes.	64
Figure 22. Raman spectrum of the NaNO_2 oriented single crystal as portrayed in Figures 17-20 recorded at 458 K using the blue 4880 Å line. $\nu_{\text{initial}} = 30 \text{ cm}^{-1}$. The ν_3 TO mode is positioned at 1250 cm^{-1} in the paraelectric, disordered phase.	66
Figure 23. Reduced, $R(\omega)$, Raman spectra of the low frequency region of NaNO_2 oriented single crystal as it went through the order/disorder phase transition. Spectra were recorded using the blue Å line at: A) 298 K; B) 383 K; C) 413 K; D) 434 K; and E) 458 K. $\nu_{\text{initial}} = 30 \text{ cm}^{-1}$. Crystal orientation is $y(xz)x$ where x and y are 110 planes.	68
Figure 24. Temperature dependence of ν_1 and ν_2 frequencies and halfwidths for NaNO_2	74
Figure 25. Intensity of LO mode for NaNO_2 recorded at 1355 cm^{-1} using the blue 4880Å line. The sample was cooling.	78
Figure 26. Raman spectrum of KNO_2 III recorded at 77 K using the blue 4880 Å line. $\nu_{\text{initial}} = 20 \text{ cm}^{-1}$. This is an ordered phase.	82
Figure 27. Raman spectra of KNO_2 as it went through the III/II, order-disorder phase transition at 264 K. The spectra were recorded using the blue 4880 Å line at: A) 102 K; B) 127 K; C) 152 K; D) 177 K; E) 202 K; F) 227 K; G) 252 K; and H) 273 K. $\nu_{\text{initial}} = 20 \text{ cm}^{-1}$	84
Figure 28. Raman spectra of the low frequency region of KNO_2 as it went through the III/II order-disorder phase transition. Spectra were recorded using the blue 4880 Å line at: A) 77 K; B) 152 K; C) 202 K; D) 252 K; and E) 273 K.	86
Figure 29. Raman spectra of KNO_2 II recorded at 298 K using the blue 4880 Å line. $\nu_{\text{initial}} = 87.0 \text{ cm}^{-1}$. This is the disordered phase.	88
Figure 30. Raman spectrum of KNO_2 I at 630 K, in the reported high temperature phase. The spectrum is simply that of the room temperature phase (II). Spectrum was recorded using the 4880 Å line. $\nu_{\text{initial}} = 50 \text{ cm}^{-1}$	90

Figure 31. Intensity, $I(\omega)$, Raman spectra of KNO_2 melt recorded at 703 K using the blue 4880 Å line. $\nu_{\text{initial}} = 30 \text{ cm}^{-1}$	92
Figure 32. Reduced, $R(\omega)$, Raman spectra of KNO_2 melt recorded at 703 K using the blue 4880 Å line. $\nu_{\text{initial}} = 30 \text{ cm}^{-1}$	94
Figure 33. Temperature dependence of ν_1 and ν_2 frequencies and halfwidths for KNO_2	99
Figure 34. Raman spectrum of RbNO_2 II recorded at 84 K using the blue 4880 Å line. $\nu_{\text{initial}} = 30 \text{ cm}^{-1}$. This is the low temperature ordered phase.	105
Figure 35. Raman spectrum of RbNO_2 I recorded at 298 K using the blue 4880 Å line. $\nu_{\text{initial}} = 30 \text{ cm}^{-1}$. This is the disordered phase.	107
Figure 36. Raman spectra of RbNO_2 as it went through the order-disorder phase transition (~ 224 K). The spectra were recorded using the blue 4880 Å line at: A) 84 K; B) 184 K; C) 209 K; and D) 235 K. $\nu_{\text{initial}} = 30 \text{ cm}^{-1}$	109
Figure 37. Raman spectrum of NO_3^- impure RbNO_2 recorded at 91 K using the blue 4880 Å line. $\nu_{\text{initial}} = 20 \text{ cm}^{-1}$. The nitrite occupies two sites as seen by the doublet at 802.5 and 814.0 cm^{-1} . Not completely ordered.	111
Figure 38. Raman spectra of NO_3^- impure RbNO_2 as it went through the order-disorder phase transition. Spectra were recorded using the blue 4880 Å line at: A) 91 K; B) 166 K; C) 216 K; and D) 241 K. $\nu_{\text{initial}} = 30 \text{ cm}^{-1}$	113
Figure 39. Raman spectrum of RbNO_2 recorded at 670 K using the blue 4880 Å line. $\nu_{\text{initial}} = 50 \text{ cm}^{-1}$. This is the disordered room temperature phase.	115
Figure 40. Intensity, $I(\omega)$, Raman spectra of RbNO_2 melt recorded at 703 K using the green 5145 Å line. $\nu_{\text{initial}} = 54 \text{ cm}^{-1}$	117
Figure 41. Reduced, $R(\omega)$, Raman spectra of RbNO_2 melt recorded at 703 K using the green 5145 Å line. $\nu_{\text{initial}} = 54 \text{ cm}^{-1}$	119
Figure 42. Temperature dependence of ν_1 and ν_2 frequency and halfwidth for RbNO_2	123

Figure 43. RbNO ₂ peak being monitored through phase transition. . . .	125
Figure 44. Temperature dependence of ν_1 and ν_2 frequency and halfwidth for impure RbNO ₂	128
Figure 45. Raman spectrum of CsNO ₂ II recorded at 83 K using the blue 4880 Å line. $\nu_{\text{initial}} = 20 \text{ cm}^{-1}$. This is the low temperature ordered phase.	133
Figure 46. Raman spectrum of CsNO ₂ I recorded at 298 K using the blue 4880 Å line. This is the disordered phase.	135
Figure 47. Raman spectra of CsNO ₂ as it went through the order-disorder phase transition ($\sim 193 \text{ K}$). Spectra were recorded using the blue 4880 Å line at: A) 83 K; B) 183 K; C) 208 K; and D) 233 K. $\nu_{\text{initial}} = 20 \text{ cm}^{-1}$	137
Figure 48. Raman spectra of the ν_2 mode as it went through the order-disorder phase transition at about 193 K. Conditions as specified in Figure 47 except for the temperatures A) 83 K, B) 183 K, C) 208 K, and D) 233 K ν_2 for RbNO ₂ at 183 K and 208 K was curve resolved into two Lorentzian components.	139
Figure 49. Raman spectrum of CsNO ₂ I recorded at 650 K using the blue 4880 Å line. $\nu_{\text{initial}} = 50 \text{ cm}^{-1}$. The spectrum is that of the disordered room temperature phase.	141
Figure 50. Intensity, $I(\omega)$, Raman spectra of CsNO ₂ melt recorded at 783 K using the blue 4880 Å line. $\nu_{\text{initial}} = 40 \text{ cm}^{-1}$	143
Figure 51. Reduced, $R(\omega)$, Raman spectra of CsNO ₂ melt recorded at 783 K using the blue 4880 Å line. $\nu_{\text{initial}} = 40 \text{ cm}^{-1}$	145
Figure 52. Temperature dependence of ν_1 and ν_2 frequency and halfwidth for CsNO ₂	149
Figure 53. Reduced, $R(\omega)$, Raman spectra of NaNO ₂ melt recorded at 573 K using the green 5154 Å line. $\nu_{\text{initial}} = 44 \text{ cm}^{-1}$. (A) $I_{\text{iso}} = I_{\parallel} - 1.3I_{\perp}$. (B) $I_{\text{aniso}} = I_{\perp}$	156

List of Tables

	Page
Table 1. Crystal Properties of Alkali Metal Nitrites.	4
Table 2. Enthalpies and entropies of the Phase Transitions in Alkali Metal Nitrites.	5
Table 3. Peak Frequencies and Halfwidths for Lithium Nitrite at Various Temperatures s = strong, w = weak, m = medium, sp = sharp, br = broad.	39
Table 4. Peak Frequencies (in cm^{-1}) for TO Modes for the Different Phases of Sodium Nitrite.	69
Table 5. Peak Frequencies and Halfwidths of ν_1 and ν_2 for Sodium Nitrite at Various Temperatures.	70
Table 6. Assignment of Normal Modes of Vibration in NaNO_2	72
Table 7. Peak Frequencies (in cm^{-1}) for the Different Phases of Potassium Nitrite.	96
Table 8. Peak Frequencies and Halfwidths of ν_1 and ν_2 for Potassium Nitrite at Various Temperatures.	97
Table 9. Peak Frequencies (in cm^{-1}) for the Different Phases of Rubidium Nitrite.	120
Table 10. Peak Frequencies and Halfwidths of ν_1 and ν_2 for Rubidium Nitrite at Various Temperatures.	121
Table 11. Peak Frequencies (in cm^{-1}) for the Different Phases of Cesium Nitrite.	146
Table 12. Peak Frequencies and Halfwidths of ν_1 and ν_2 for Cesium Nitrite at Various Temperatures.	147

Table 13. Peak Frequencies and Halfwidths for Aqueous KNO_2	153
Table 14. Peak Frequencies and Halfwidths for Molten Alkali Metal Nitrites.	154
Table 15. Alkali Metal Nitrite Melts. Depolarization Ratios and Integrated Intensity Ratios.	159
Table 16. Polarizability Anisotropies for Nitrites and Other Oxyanion Systems.	160

ABSTRACT

The alkali metal nitrites have been studied from 77 K through the phase transitions and in the molten state by Raman spectroscopy. With the exception of LiNO_2 , all the alkali metal nitrites go through at least one solid-solid phase transition. The presence of NO_2^- groups disordered over non-equivalent crystallographic sites is a common feature of at least one phase for each salt.

The results for LiNO_2 are not consistent with the suggested D_{3d}^5 crystal structure. Spectroscopic evidence and ab initio calculations indicated that the NaNO_2 order-disorder transition occurs via a nitrite rotation about the crystallographic *a* axis. No evidence was obtained for the reported phase transitions at 343 or 380 K in KNO_2 or for the high temperature phase transition in CsNO_2 . For RbNO_2 , the effect of nitrate impurity was considered. The spectroscopic observables are discussed in relation to available thermodynamic quantities.

INTRODUCTION

The alkali metal nitrites have attracted much interest in recent years for both practical and theoretical reasons. These salts give low melting nitrite-nitrite and nitrite-nitrate eutectic mixtures, therefore they have a potential use as electrolytes in molten salt thermal batteries and as heat exchange media in nuclear reactors. Interest in their bonding habits has been enhanced by Hathaway and Slade (1966)¹ who discovered two possible forms of the nitrite ligand (nitro and nitrito) in transition metal complexes. Further, three of the salts, KNO_2 , RbNO_2 and CsNO_2 , are believed to possess plastic crystal properties.² Interest in N-O vibrations of ions similar to nitrate has also focused attention on metal nitrites.^{3a} Probably the greatest interest in the alkali metal solids stems from the fact that they exhibit order-disorder phase transitions. In fact, this has spurred much of the study of NaNO_2 which has a ferroelectric to paraelectric phase transition and an incommensurate intermediate phase.^{3b} With the exception of NaNO_2 , and to a lesser extent KNO_2 , nitrites have not been previously studied in great detail, unlike the corresponding nitrates. This is due mainly to the difficulty in preparing pure solids.^{3c}

The purpose of this study was to prepare pure alkali metal nitrites and analyze them in all solid phases and in the molten phase using Raman spectroscopy. The study of order-disorder phase transitions in relatively simple solids will assist in the understanding of the transitions in more complex solids. Characterization of these salts by their spectra will be useful in future studies of reactions of nitrites. Finally, attention has been focused on the similarities and differences between the nitrite and nitrate systems, particularly for the melts. Since the nitrates have been well studied, this comparison may aid in understanding or predicting properties of the nitrite. Furthermore nitrate is a common impurity in nitrites.^{3c}

The solid phases and the phase transitions of the nitrites have been examined in some detail. Available crystallographic data is presented in Table 1, while available data for the known transitions in the alkali metal nitrites is summarized in Table 2. Known thermodynamic data relating to the phase transitions are included in this table.

No conclusive structural studies of anhydrous LiNO_2 have been reported, however Wyckoff has proposed a unimolecular cell of space group $D_{3d}^5 (R_{3m})$.⁴ The crystal structure of the monohydrate is known.¹⁸ Lithium nitrite has been the subject of very few spectroscopic studies^{19,20,21} due mainly to the difficulty in preparing a pure sample. The Raman spectra obtained in this investigation are consistent with those of previous spectroscopic studies while this study is extended to include spectra of the melt. The spectra presented indicate LiNO_2 is an ordered solid but they are not consistent with the suggested crystal structure.

Sodium nitrite has been the subject of extensive experimental and theoretical investigations.^{3b} Recent interest in order-disorder transitions, particularly as related to ferroelectrics, has led to many studies on NaNO_2 because it is a ferroelectric²²; it has a relatively simple crystal structure in both its ordered and disordered phases; it exists as a stable, pure compound; and its order-disorder phase transition occurs at an easily obtainable temperature, ~ 435 K. The presence of an incommensurate antiferroelectric phase^{6a} between the room-temperature ordered ferroelectric and high-temperature paraelectric phases has sparked even further interest in the research on NaNO_2 .

The mechanism for the order-disorder transition in NaNO_2 is a contentious issue. While spectroscopic^{13b,23-28} and optical measurements^{29,30,31} indicated that the order-disorder transition involved rotation of the NO_2^- ion about the crystallographic a axis; theoretical^{31,32} and molecular dynamics calculations^{33,34} indicated that the rotation about the crystallographic c axis was more probable. Neutron

Table 1. Crystal Properties of Alkali Metal Nitrites.

	Phase	Symmetry	Z	Configurational entropy	Reference
LiNO ₂	c	(maybe D _{3d} ⁵ , R _{3m})	1 or 3	ordered	4
NaNO ₂	c, III, Bodycentered	C _{2v} ²⁰ (I _{m2m})	1	ordered	4,5
	c, II, incommensurate		~ 10	disordered	6a
	c, I, orthorhombic	D _{2h} ²⁵ (I _{mmm})	2	Rln2	6b
KNO ₂	c, VII, Monoclinic	C ₂ ² or C _{2h} ² (P _{2i} or P _{2i/m})	4	ordered	7
	III, Monoclinic	C _{2h} ⁵ (P _{2i/c})	4	ordered	7
	II, Rhombohedral	D _{3d} ⁵ (R _{3m})	3	Rln12	8
	I, Face-centered cubic	O _h ⁵ (F _{m3m})	4	Rln32	9
	II, Monoclinic	C _{2h} ³ (B _{2/m} or C _{2/m})	4	ordered	2
RbNO ₂	I, Face-centered cubic	O _h ⁵ (F _{m3m})	4	Rln32	10
	II, Rhombohedral	D _{3d} ⁵ (R _{3m})	1	Rln3	10
CsNO ₂	I, Body-centered cubic	O _h ¹ (P _{m3m})	1	Rln12	2,10

Table 2. Enthalpies and Entropies of the Phase Transitions in Alkali Metal Nitrites.

Alkali Metal	Phase Transition	T/K	$\Delta H_p/kJ\cdot mol^{-1}$	$\Delta S_p/JK^{-1}mol^{-1}$	Reference
Li	c \rightarrow I	493			11,12
Na	III \rightarrow II	436	1.19	2.75	13a,13b
	II \rightarrow I	439			
	I \rightarrow I	551	13.3	24.2	2
K	VII \rightarrow III	230	-	-	7
	III \rightarrow II	264.1	5.048	23.54	14
	II \rightarrow I	314.7	2.107	7.01	14
	I \rightarrow I	665	6.98	10.5	2
Rb	II \rightarrow I	$263.7 \pm .2$	8.494	32.3	15
	I \rightarrow I	695	6.53	9.40	2
Cs	II \rightarrow I	208.85	2.762	13.28	17
	II \rightarrow I	$209.16 \pm .10$	3.45 ± 0.2	17.2 ± 1.0	16
	I \rightarrow I	673	9.22	13.7	2

diffraction^{35,36,37}, X-ray^{37,38}, and an ²³Na nmr study³⁹ all supported the latter theory. However most of the evidence in favour of c axis rotation was based on model calculations with hard-sphere potentials that neglected the large non-bonded electron density at the N atom. Analysis of all available data in addition to the present spectroscopic observations and an ab initio study (the details of which are included in this work as an appendix) lead to the conclusion that the orientational disorder of NO₂⁻ ions is more probably realized by rotation about the crystallographic a axis.

Potassium nitrite has been studied to a lesser extent; the solid is extremely hygroscopic, has a high melting point (665 K), and decomposes readily above the melting point. At room temperature it takes the form of an unmanageable plastic. In addition, KNO₂ is known to form a solid solution with NO₃⁻, therefore purification becomes very difficult.^{3c,20}

The polymorphism of KNO₂ is much more complex than that of NaNO₂. Currently there are nine known phases which have all been identified by Raman and mid-infrared spectroscopy.⁴⁰ Seven of these phases have been characterized by x-ray powder photography, but structural interpretation of the x-ray data remains unsettled. Of the nine known phases, only four are stable at ambient pressure, KNO₂ I, II, III and VII. The five high-pressure phases thought to be related to the CsCl form have also been studied⁴¹ but will not be discussed in this work.

While some x-ray studies indicate KNO₂ III is ordered⁷, a recent spectroscopic study⁴⁰ indicates it is more likely to be disordered. The present investigation suggests some order remains in this phase. In addition this study supports the III/VII phase transition at 230 K^{7,40} but shows no evidence for reported phase transitions at about 343 K⁴² or 380 K⁴³. There have been many ir and Raman spectroscopic studies^{19,20,21,40,43} of KNO₂ reported but none have involved a detailed investigation of the solid to the melting point prior to this work. No phase transition was observed

between the II/I transition and the melting point. The present spectral data are consistent with available thermodynamic data.

Rubidium and cesium nitrite are very much like potassium nitrite; they are extremely hygroscopic, hard to purify, have high melting points, easily decompose, and form unmanageable plastic solids.^{2,20}

The polymorphism in rubidium nitrite has been studied by several workers^{2,10,15} and the crystal structure of at least two polymorphs of the salt have been determined. There are many discrepancies in the reported phase transitions however. The II/I transition has been observed to occur at about 264 K by several workers^{2,15,45} while a temperature of 252 K has also been suggested.¹⁰ In addition, transitions have been reported to occur at 360 K⁴⁴ and 340 K¹⁵ and minor anomalies at 225-249 K and 400-415 K.¹⁵ There was no evidence for the high-temperature phase transitions at 340 or 360 K in this investigation. However, new evidence is presented for a phase transition at about 225 K which coincides with a minor anomaly observed by calorimetric studies. It is important to note the only previously reported Raman spectroscopic data for RbNO₂ has been that of the fused salt.²¹ The present investigation provides the first spectroscopic study of the phases in RbNO₂ solid.

The polymorphism of cesium nitrite also remains unsettled. Two solid phases have been characterized, and both are believed to be disordered. Many transition temperatures have been reported, 175 K⁴⁵, 179 K¹⁰, 209 K^{10,17}, 353 K⁴⁵, 365 K⁴⁴ and 393 K¹⁵, based on dta, conductivity and calorimetric measurements. Raman spectra obtained in this investigation indicates only one solid-solid phase transition exists - that of about 209 K. Cesium nitrite has been the subject of very few vibrational spectroscopic investigations.^{16,19-21} A detailed study covering all the phases of CsNO₂ has not been done before this investigation.

In the present study, LiNO_2 , NaNO_2 , KNO_2 , RbNO_2 and CsNO_2 , have been characterized from 77 K through the phase transitions and in the molten state using Raman spectroscopy. The melts have been studied for comparison with the high temperature disordered phases and for comparison with other systems such as the nitrates. Finally, the details of an ab initio study which support some of the spectroscopic data are presented as an appendix. The ab initio calculations include optimized geometries for nitro and nitrito forms of the nitrites, the polarizability of nitrito NaNO_2 along the a, b and c axes, and the energy potentials for the nitrite rotation about the a and c axes in NaNO_2 .

THEORY

Non-Interacting Molecules

Radiation interacts with matter through the dipole moment vector, μ , which is composed of a permanent part, μ^P , and an induced part, μ^i (see Refs. 46 and 47).

$$\mu = \mu^P + \mu^i \quad (1)$$

Light of a given polarization may impinge on a molecule to give the induced dipole moment which subsequently radiates. For linear or spontaneous Raman scattering, only the first order term in applied electric field vector, E , need be considered.

$$\mu^i = \underline{\alpha}E \quad (2)$$

Higher terms in E^n must be included for non-linear processes.⁴⁷ The induced dipole moment vector, μ^i will not generally be parallel to the applied field vector, E , particularly for crystals. Consequently, the polarizability, $\underline{\alpha}$, will be a symmetric tensor

$$\underline{\alpha} = \begin{pmatrix} \alpha_{xx} & \alpha_{xy} & \alpha_{xz} \\ \alpha_{yx} & \alpha_{yy} & \alpha_{yz} \\ \alpha_{zx} & \alpha_{zy} & \alpha_{zz} \end{pmatrix} \quad (3)$$

Both μ^P and μ^i have a static contribution due to the equilibrium molecular structure and a dynamic contribution due to changes in these properties associated with the (3N-6) normal modes of vibration.

$$\mu^P = \mu_o + \sum_i^{3N-6} \frac{\partial \mu}{\partial Q_i} Q_i \quad (4)$$

$$\underline{\alpha} = \underline{\alpha}_o + \sum_i^{3N-6} \frac{\partial \underline{\alpha}}{\partial Q_i} Q_i \quad (5)$$

Here Q_i are the 3N-6 vibrational normal coordinates of the molecule. Since infrared processes are governed by eqn. (4) and light scattering (Raman and Rayleigh) are

governed by eqn. (5), the two spectroscopies are quite complementary and should normally be considered together. The predicted number, symmetry and activity of the 3N-6 infrared and Raman modes for a given molecular geometry can be deduced from group theoretical rules as explained by Cotton⁴⁸ or Ross⁴⁹.

The polarizability tensor $\underline{\alpha}$ is often considered to be comprised of a symmetric part described by the mean polarizability invariant, α ,

$$\alpha = \frac{1}{3} (\alpha_{xx} + \alpha_{yy} + \alpha_{zz}) = \frac{1}{3} \text{Tr } \underline{\alpha} \quad (6)$$

and an asymmetric part described by the mean polarizability anisotropy, β , defined as

$$\beta = \frac{1}{2} [(\alpha_{xx} - \alpha_{yy})^2 + (\alpha_{yy} - \alpha_{zz})^2 + (\alpha_{zz} - \alpha_{xx})^2 + 6(\alpha_{xy}^2 + \alpha_{yz}^2 + \alpha_{zx}^2)]^{\frac{1}{2}} \quad (7)$$

A set of axes in the free molecule can always be found, such that, with these axes as the basis vectors, the polarizability tensor has only diagonal elements and the expression for β greatly simplifies. Along these axes, called the principal axes *c.f.* the polarizability, μ^i and E have the same direction. The principle axes define an ellipsoid which will have the same symmetry as the charge distribution and will normally be the symmetry defined by the nuclear positions. The polarizability is isotropic when the static polarizability anisotropy equals zero ($\beta = 0$), as for a spherical top molecule like CCl_4 . It is anisotropic when two or more axes are different ($\beta > 0$).

The quantum mechanical expression in the Schrodinger representation⁵⁰ for the differential scattering cross section into a solid angle, Ω and frequency range, $d\omega$ about ω_0 is

$$\frac{d^2\sigma}{d\Omega d\omega} = \lambda_s^{-4} \sum_{i,f} | \langle i | \hat{\epsilon}_i \underline{\alpha} \cdot \hat{\epsilon}_s | f \rangle |^2 \rho_f \delta(\omega_0 - \omega_f) \quad (8)$$

where

λ_s the wavelength of scattered light divided by 2π

- $E_i E_s$ unit vectors defining the polarization direction
of the initial and scattered light
- α polarizability tensor of the scattering medium
- i, f initial and final states of the system with energies
 E_i and E_f
- $\hbar\omega_{i,f}$ $E_f - E_i$
- ρ_i probability that the system is in initial state

If $E_f > E_i$, Raman lines occur at lower frequencies (Stokes lines) than the incident exciting line whereas, if $E_f < E_i$ the Raman lines occur at higher frequencies (anti-Stokes lines) than the incident exciting line. Normally, the Stokes spectrum is measured since it gives more intense lines.

Experimentally and theoretically, the scattered light intensity may be divided into two parts, polarized and depolarized. When E_f and E_s are perpendicular only the depolarized component appears (eqn. 9) and when E_f and E_s are parallel both components appear (eqn. 10).

$$\frac{d^2\sigma \text{ depol}}{d\Omega d\omega} \equiv 1/10 \frac{d^2\sigma}{d\Omega d\omega_{\perp}} \quad (9)$$

$$\frac{d^2\sigma \text{ pol}}{d\Omega d\omega} \equiv \frac{d^2\sigma}{d\Omega d\omega_{\parallel}} + \frac{4}{3} \frac{d^2\sigma}{d\Omega d\omega_{\perp}} \quad (10)$$

These equations are normally written in terms of intensities:

$$I_{\sigma}(\omega) = I_{\text{iso}}(\omega) = I_{\text{pol}}(\omega) = I_{\parallel}(\omega) - \frac{4}{3} I_{\perp}(\omega) \quad (11)$$

$$I_{\beta}(\omega) = I_{\text{anis}}(\omega) = I_{\text{dep}}(\omega) = I_{\perp}(\omega) \quad (12)$$

Where I_{\parallel} and I_{\perp} are measured and I_{iso} must be calculated. Normally I_{\parallel} is measured with the incident laser light and the analyzed scattered light both polarized in the vertical plane, whereas I_{\perp} is measured with the incident laser light polarized in

the vertical plane but the scattered light is analyzed for the horizontal plane.

If α and β are expanded in the vibrational normal coordinates of a molecule and only the linear terms are kept then eqn. (5) leads to

$$\alpha \mathbf{1} = \alpha_0 \mathbf{1} + \sum_i \left[\frac{\partial \alpha \mathbf{1}}{\partial Q_i} \right] Q_i + \dots \quad (13)$$

$$\beta = \beta_0 + \sum_i \left[\frac{\partial \beta}{\partial Q_i} \right] Q_i + \dots \quad (14)$$

where $\mathbf{1}$ is the unit tensor, and α_0, β_0 are the isotropic and anisotropic components of the molecular polarizability tensor evaluated at the equilibrium internuclear separation. The α_0, β_0 terms give rise to the polarized and depolarized Rayleigh scattering and rotational Raman scattering centered about zero frequency, which occurs without change in the vibrational coordinates of the molecule, and $\omega_{\text{R}} = 0$. The terms dependent on the normal coordinates give rise to Raman scattering. Since $\frac{\partial \alpha \mathbf{1}}{\partial Q_i}$ is independent of molecular orientation the $I_{\alpha}(\omega)$ Raman spectrum is dependent only on vibrational motion. However, $\frac{\partial \beta}{\partial Q_i}$ also depends on molecular reorientation, therefore I_{β} depends on both vibrational and reorientational motions of the molecule. In addition to the familiar qualitative use of the depolarization ratio, $\rho = \frac{I_{\perp}}{I_{\parallel}}$ to identify symmetric modes (i.e. $\rho < 0.75$), the quantitative studies of I_{α} and I_{β} may provide detailed information about vibrational and reorientational relaxation.

Information related to vibrational and reorientational relaxation processes can be obtained by band shape analysis through time correlation function methods of Gordon^{51,46,47}. A semi-quantitative understanding of the origins of bandwidths can be achieved without rigorous calculation of correlation functions. Although the various correlation times can be obtained from the integration (eqn. 15) very good approximations of the correlation times can be obtained from the full widths at half

height of the band.⁵¹

$$\tau = \int_{-\infty}^{\infty} G(t) dt \quad (15)$$

where $G(t)$ is an auto correlation function defined as

$$G(t) = \langle A(0) \cdot A(t) \rangle \quad (16)$$

and $A(t)$ are dynamical quantities defined in such a way as to make the ensemble average of $A = 0$. If $G(t)$ is an exponentially decaying function of time

$$G(t) = A \exp \frac{-t}{\tau} \quad (17)$$

then the band profile in frequency space will have a Lorentzian shape with full width and half height, Γ (in cm^{-1}) given by

$$\Gamma^{-1} = \pi c \tau \quad (18)$$

Even though bands are often not exactly Lorentzian especially in the far wings, the τ values are not significantly different from those obtained by integration of the correlation function. For example, if one chooses a totally symmetric vibration with a low depolarization ratio, then the vibrational and reorientational relaxation times τ_v and τ_R can be determined from the halfwidths of the isotropic and anisotropic spectrum:

$$\Gamma_{\text{iso}} = \Gamma_v = \Gamma_{\parallel} \quad (19)$$

$$\Gamma_{\text{aniso}} = \Gamma_{\perp} = \Gamma_v + \Gamma_R \quad (20)$$

$$\frac{1}{\tau_v} = \pi c \Gamma_v \quad (21)$$

$$\frac{1}{\tau_R} = \pi c \Gamma_R = \pi c (\Gamma_{\perp} - \Gamma_{\text{iso}}) \quad (22)$$

When the halfwidth of the anisotropic spectrum is greater than that of the isotropic

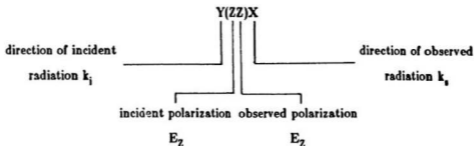
spectrum the difference can be ascribed to reorientational relaxation and used to measure Γ_R since the width of the isotropic component is only due to vibrational relaxation. Similarly, if the infrared halfwidth for the same peak can be measured, then an approximate measure of the halfwidth of the infrared band due to reorientational effect can be obtained by subtracting the halfwidth of the isotropic Raman from the total infrared halfwidth.

Crystals

Raman spectroscopy of crystals involves the inelastic scattering of photons whereby the energy lost or gained by the photons is used to create or annihilate phonons in the crystals. An ordered crystal may be viewed as a large number of repeat units related by translational symmetry. If there are n atoms in each unit cell (n about 10-20 for simple inorganic salts) and N unit cells in a piece of crystal (N about 6.0×10^{23}) there will be $3(nN) - 3$ or $\sim 10^{24}$ normal modes of vibration. These normal modes of vibration may be treated as standing plane waves and are called phonons. Fortunately the conservation of wave vector, κ (pseudo momentum) dictates that only motions in phase from unit-cell to unit-cell are observed by infrared and Raman spectroscopy, i.e. κ about 0. The $\kappa = 0$ selection rules for crystals may be deduced for known structures through group theory of unit cell symmetry⁵² or by correlation methods^{53,54}. For a crystal which contains molecules or molecular ions the normal modes of vibration will be comprised of internal modes (stationary centre of mass motions of the molecule) and external Rotatory and Translatory modes which involve relative motions of the molecules or ions of the unit-cell. There will also be three acoustic phonons at zero wavenumber.

In a crystal the polarizability is fixed in space and the six independent polarizability tensor components (Eq. 3) α_{xx} , α_{yy} , α_{zz} , α_{xy} , α_{xz} and α_{yz} may be defined with respect to the crystallographic axes. The six independent components of the derived polarizability tensor may be obtained by observing the Raman scattering from a

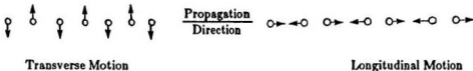
crystal oriented in different directions. Porto's method of designating the crystal and polarization directions is widely used by Raman spectroscopists⁵⁵



The letters in parentheses give the components of the derived polarizability tensor that are measured by the observation, for the example in the case shown, α'_{zz} .

Important information concerning molecular environments in crystals may also be obtained from Raman spectroscopic measurements. For example, the presence of transverse optical (TO) longitudinal optical (LO) mode pairs in the spectra of solids can establish that a crystal has no centre of symmetry and may be piezoelectric. Normal modes in a crystal (phonons) have a defined propagation direction, and LO modes are those which have an electric vector parallel to the propagation direction, singly degenerate. The regularly occurring TO modes have electric vectors perpendicular to the propagation direction and are therefore doubly degenerate. These motions are represented in figure 1.

Figure 1. Motions in a One-Dimensional Crystal



In Raman and infrared spectroscopic studies the active LO and TO modes are those

for which the wave vector, k , approaches zero. That is, the motions are in phase throughout the unit cells of the crystal.

Longitudinal optic modes are only Raman active for non-centrosymmetric crystals. This stems from the fact that the origin of LO modes rests in a dipole moment change with a perpendicular phonon. Thus for centrosymmetric crystals, the mutual exclusion rule applies, preventing Raman active LO modes.

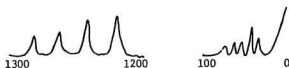
The motion of oppositely charged ions against one another in LO modes means there is a higher restoring force for the motion, therefore LO modes are often peaks at highest energy in a vibrational spectrum. The exact energy or frequency of LO modes may depend on the propagation direction of the exciting wave. LO modes show a pronounced orientational dependence for non-centric crystals with low symmetry. This means that the LO peaks tend to be at different frequencies for different geometries for low symmetry crystals. New optical modes can be made observable or old ones disappear by changing the direction of incident radiation with respect to the crystal since motions in a different direction through the crystal are excited by the light. It is theoretically possible to determine relative molecular positions and thus space groups as well as coupling constants between atoms or molecules in a crystal by studying LO modes therefore.

Raman spectroscopic measurements can also detect ionic disorder in solids. In a vibrational spectrum, a density of states is observed; that is the spectrum plots the frequencies for every vibration of every molecule in the crystal. In disordered solids there is no intermolecular coupling and each molecule acts almost independently. The phonons of a branch have similar energy over a continuous distribution and bands, not lines are observed. These bands actually represent a range of frequencies of all the vibrational modes over a range of environments. For a disordered solid, such as paraelectric NaNO_2 where the NO_2^- ions are continuously reorienting the molecular dipole in the plane of symmetry, there is no long-range symmetry within

the crystal. The frequencies of a given vibrational mode therefore will vary greatly and give rise to a broad band. In an ordered solid however, there is long-range symmetry and the intermolecular coupling from unit-cell to unit-cell throughout the crystal imposes structure on the density of states. This means there will be a number of bands at different given frequencies over the density of states. Thus the spectra of ordered and disordered solids will look like those depicted in figure 2.

Figure 2. Comparison of Vibrational Spectra for Ordered and Disordered Solids.

ordered solid



disordered solid



Data Treatments

Important information may also be obtained from relative Raman intensities and normalized forms of the intensity⁴⁶. The integrated Raman intensity, $I_{(i)}$, for the i^{th} normal mode of vibration is defined by:

$$I_{(i)} = \int_{\text{band}} I(\omega) d\omega \quad (23)$$

where $I(\omega)$ is the point intensity at each wavenumber over the band. In the double harmonic approximation the molar scattering activity $S_{(i)}$ for the i^{th} normal mode is given by⁴⁷:

$$I_{(i)} = C(\omega_0 - \omega_i)^4 \omega_i^{-1} B^{-1} S_i \quad (24)$$

where

C Constant

ω_i Harmonic frequency of the normal mode

B is a temperature factor for which the Boltzman distribution gives a good approximation

$$B = (1 - e^{-hc\omega/kT}) \quad (25)$$

The relationship expressed in eqn. 24 assumes that $I_{(i)}$ is independent of the incident light frequency, ω_o (i.e. no resonance Raman effect) and intensity, E (i.e. no non-linear effects).

The quantity of real interest in the Raman experiment is the molar scattering efficiency $S_{(i)}$ given by $(\frac{\partial\alpha}{\partial Q_i})^2$. It is convenient to construct a normalized or reduced intensity spectrum, $R(\omega)$ such that band areas in $R(\omega)$ will give relative values of $S_{(i)}$ directly. Corrections for the frequency dependence of instrument response and for slit distortion may be included in $R(\omega)$ as required.

$$R_{(\omega)} = I_{(\omega)} \cdot (\omega_o - \omega_i)^{-4} \cdot \omega \cdot B \quad (26)$$

$$S_{(i)} = \int_{\text{band}} R_{(\omega)} d\omega \quad (27)$$

Reduced spectra of this type are often used in the low-frequency region where the effect of temperature is most pronounced. One of the biggest advantages of the $R(\omega)$ spectrum is that it removes the effect of the Rayleigh scattering at low frequencies. The $R(\omega)$ spectrum has the same functional form as the infrared absorption coefficient^{56,57} and has been described as the energy absorbed in a scattering process or as a measure of the vibrational density of states.⁵⁷ Theoretically the values of $S_{(i)}$ can be used to provide information about electron distribution in a chemical bond.⁵⁸

It has been suggested that when a bond X-Y stretches the only change in molecular polarizability is localized in the bond and α_{XY} is a bond property.

EXPERIMENTAL

Preparation of the alkali metal nitrites

LiNO_2 was prepared by stoichiometric addition of $\text{Li}_2\text{SO}_4 \cdot \text{H}_2\text{O}$ to $\text{Ba}(\text{NO}_2)_2$. The insoluble BaSO_4 was filtered off and the resultant solution analysed to ensure no excess SO_4^{2-} remained. The yellow LiNO_2 solution was treated with activated charcoal to remove fluorescing impurities, and was slowly (~ 7 days) evaporated to dryness by heating to $50\text{-}60^\circ\text{C}$. The pH of the solution was kept slightly basic (pH ~ 8) throughout the process, by the addition of LiOH when necessary, since it was found the nitrite decomposed in an acid solution. The lithium salt crystallizes as the stable monohydrate, $\text{LiNO}_2 \cdot \text{H}_2\text{O}$. Anhydrous LiNO_2 was obtained by carefully drying the hydrate under vacuum in a quartz tube; the temperature was slowly (1-2 days) increased to 110°C and the sample left for a further 2-3 days to dry. The sample was stored in a vacuum desiccator.

KNO_2 was prepared in a similar manner from K_2SO_4 . The salt was obtained upon evaporation of the solution and dried at $\sim 110^\circ\text{C}$ for several days before being stored in a vacuum desiccator.

RbNO_2 was prepared in an analogous manner from RbOH and Rb_2CO_3 . 6M H_2SO_4 was added to the RbOH , Rb_2CO_3 mixture until a pH of ~ 8 was reached. The solution was filtered and the Rb_2SO_4 filtrate titrated against $\text{Ba}(\text{NO}_2)_2$ until no more BaSO_4 precipitated. This solution was then filtered, treated with activated charcoal and slowly (5 days) evaporated to dryness to produce RbNO_2 . This solid was also dried and stored in a vacuum desiccator.

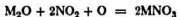
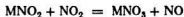
Similarly, CsNO_2 was prepared from CsSO_4 . However, the salt obtained contained considerable SO_4^{2-} and NO_3^- impurities. The impurities were removed by the ion exchange method of Ray⁹, using Dowex 1-X8, 20-50 mesh anion exchange resin. Pure CsNO_2 was obtained after just one pass through the column and once

obtained, this solid was also stored in a vacuum desiccator.

High purity reagent grade NaNO_2 (AnalaR) with a minimum nitrite assay of 98% was recrystallized from H_2O . The solution was treated with activated charcoal to remove any fluorescing impurities. Single crystals of NaNO_2 were also made. Reagent grade NaNO_2 (AnalaR) was melted in a 20 mL glass ampoule and the melt cooled at a very slow rate; 2°C per day initially to $8^\circ\text{--}10^\circ\text{C}$ per day as the sample neared room temperature. Single crystals were then cleaved from the solid and stored in a desiccator.

Sample Purity

Sample purity with nitrites can be a real problem for several reasons. It is necessary to keep the pH at approximately 7 or 8 during sample preparation since acidic conditions result in the formation of unstable nitrous acid and NO_3^- impurity while basic conditions lead to OH^- contamination and possible CO_3^{2-} impurity from dissolved CO_2 . The samples are hygroscopic and must be carefully dried. Furthermore, molten nitrites decompose very close to their melting points. Decomposition of the alkali metal nitrites leads to a loss of nitrogen oxides and formation of the nitrate salts as described by the following mechanism reactions:⁶⁷



The nitrites of K, Rb and Cs form solid solutions with dissolved nitrate^{3c,20,60} and are difficult to purify. Initial Raman spectra of the lithium and sodium solids showed a NO_3^- impurity near the detectable limit of 0.1 mol % or less as determined by the

method of Brooker and Irish^{3c}. The K, Rb and Cs solids contained an initial NO_3^- impurity of 0.55, 0.45 and 0.8 mol % respectively. Pure RbNO_2 also had a 0.16 mol % SO_4^{2-} impurity present due to the Rb_2SO_4 used in preparation of this salt. The impure RbNO_2 was found to be about 1-2 % impure with NO_3^- and 1% impure with CO_3^{2-} perhaps due to unreacted Rb_2CO_3 used in the preparation.

After these samples were melted to obtain spectra of the molten salts, the nitrate impurity increased significantly to 0.2, 0.15, 1.7, 1.2 and 1.5 mol % for Li, Na, K, Rb and CsNO_2 respectively. All the alkali metal nitrite melts decomposed but decomposition was worse for LiNO_2 and CsNO_2 . Bubble formation hindered the measurement of Raman spectra. Satisfactory spectra of molten LiNO_2 , for example, were only obtained after sealing the salt under $\text{NO}(\text{g})$ in an attempt to suppress decomposition and bubble formation. The other samples were sealed under dry N_2 to suppress bubble formation.

The impurities reported were estimated by measuring the intensities of bands due to the impurity relative to the intensity of the $\nu_2 \text{NO}_2^-$ mode. The Raman bands for NO_3^- impurity were at 1050 and 704 cm^{-1} , SO_4^{2-} at 980 cm^{-1} and CO_3^{2-} at 1060 and 684 cm^{-1} .

Instrumentation

Raman spectra were recorded on a double monochromator Coderg spectrometer using the 4880 Å or 5145 Å line of a Control argon ion laser as the source of excitation. The photon counting detection was coupled to the MUN VAX 11/780 computer, whereby several programs were used to process the spectra recorded, for example signal average multiple scans.

The spectra of the solids were obtained from dry samples sealed under vacuum, except LiNO_2 which was sealed under $\text{NO}(\text{g})$ and NaNO_2 single crystals which were not sealed. Each sample was heated under vacuum at $\sim 110^\circ\text{C}$ in 2 or 4 mm id.

quartz tubes for 2-3 days. Those samples were then melted under Ar(g) and the argon pumped off before the samples were sealed under vacuum. This process insured that the samples were absolutely water free and were indefinitely stable.

LiNO₂ and NaNO₂ were placed on the "cold finger" of a glass evaporating N₂(l) Cryostat (Figure 3a) to obtain low temperature (77 K) spectra while KNO₂, RbNO₂ and CsNO₂ were placed in a N₂(l) cooled Coderg Cryostat (Figure 3b). Spectra were recorded between 77 K and room temperature for these samples. Room temperature spectra were recorded at ambient temperatures (295-300 K), and high temperature spectra were recorded up to 15°-50° of the melting points. The samples were heated in a tube oven (Figure 4). Spectra of the melts were recorded for both polarized, I_{||} and depolarized, I_⊥ scattering geometry and I_{isotropic} was calculated from I_{iso} = I_{||} - 4/3I_⊥. Spectra are presented in both the I(ω) and R(ω) formats.

A schematic diagram of the apparatus used for obtaining Raman spectra is presented in Figure 5.

Figure 3a. Glass Evaporating $N_2(1)$ Cryostat.

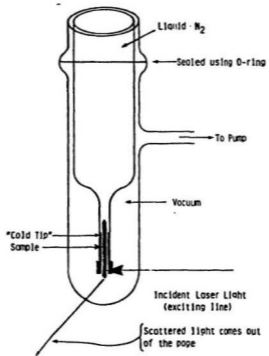


Figure 3b. Coderg Cryostat.

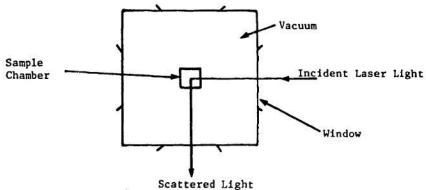
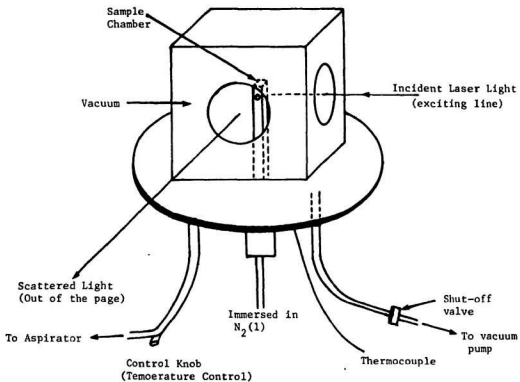


Figure 4. Oven for Obtaining High Temperature Spectra.

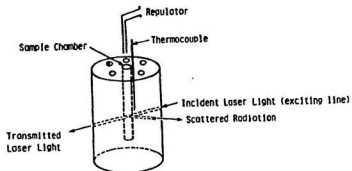
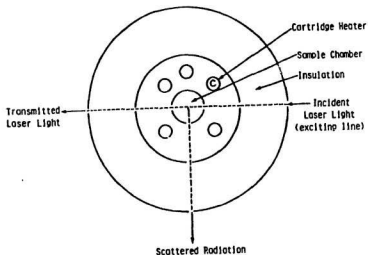
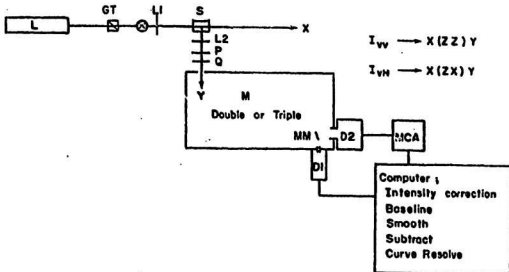


Figure 5. Schematic Representation of Apparatus used for Obtaining Raman Spectra.



where L is a laser usually Argon-ion (4880, 5145 Å) or Krypton-ion (5682, 6471 Å)

GT: Glan-Thompson prism; Used to improve polarization characteristics of the laser

⊗: Half-wave plate; Used to rotate the polarization of the laser through 90°

L1: focusing lens

S: sample. It is useful to mask the sample to reduce stray light

L2: collecting lens; Focuses the scattered light on the monochromator (m) slit through a polarization analyzer (P) and a quarter-wave plate scrambler (Q).

D1: conventional photomultiplier detector used with an exit slit

D2: Diode array Detector used with no exit slit. A large spectral region is focused on the detector at once.

D1 or D2 type detection can be used but not at the same time.

RESULTS AND DISCUSSION

LiNO₂

Lithium nitrite crystallizes from aqueous solution as the monohydrate which may be dehydrated at 383 K, but reportedly decomposes at 473 K before melting at 493 K. The crystal structure for LiNO₂ is unknown but it is believed to be an ordered solid. Wyckoff has proposed a unimolecular cell of space group $D_{3d}^5 (R_{3m})$ with $a_0 = 5.073$, $\alpha = 32^\circ 2'$ and $\mu = 0.25$.⁴

Carr et al (1979)¹⁹ have suggested there are three molecules per unit cell based on their Raman spectroscopic study over the range 18 K to 493 K. Room temperature Raman and infrared spectra were also obtained for LiNO₂ by Brooker and Irish²⁰, and infrared spectra for the temperature range 310 K to 453 K were obtained by Gafurov.⁶¹ In addition, Raman data for molten lithium nitrite was reported by Prisyazhnyi et al.²¹

In this study, Raman spectra were obtained for solid lithium nitrite over the temperature range 77 K to the melting point, and for the melt. These spectra are illustrated in Figures 6 to 10. Table 3 presents the peak frequencies and halfwidths for these spectra. All spectra recorded contain a rising baseline due to the fluorescence from the LiNO₂ sample despite attempts to remove impurities during sample preparation. This is possibly due to the presence of NO₂ produced as a decomposition product.

At 77 K (figure 6), the low frequency lattice modes are well defined, a fact which is consistent with an ordered solid. There were no sudden changes in the peak positions or halfwidths of the internal modes up to the melting point, hence there is no indication of a phase transition over this temperature range (Figures 6,7,8 and 11). In particular, there is no evidence for a phase change at 367 K as indicated in the DTA and electrical conductivity results of Protsenko et al (1971).⁴⁵ This result

Figure 6. Raman spectrum of LiNO_2 recorded at 77 K using the blue 4880 Å line.
 $\nu_{\text{initial}} = 30 \text{ cm}^{-1}$.

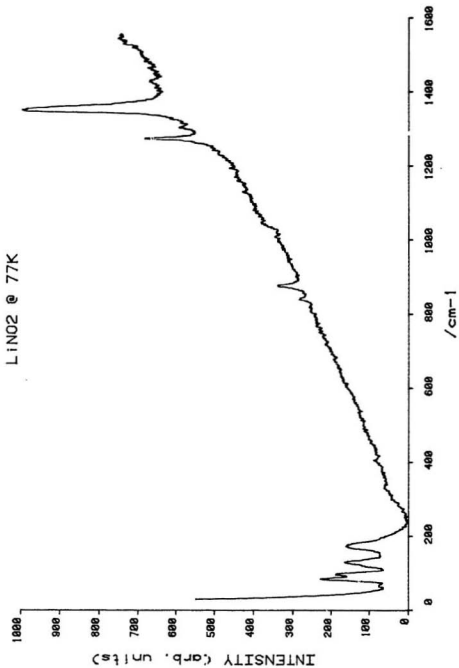
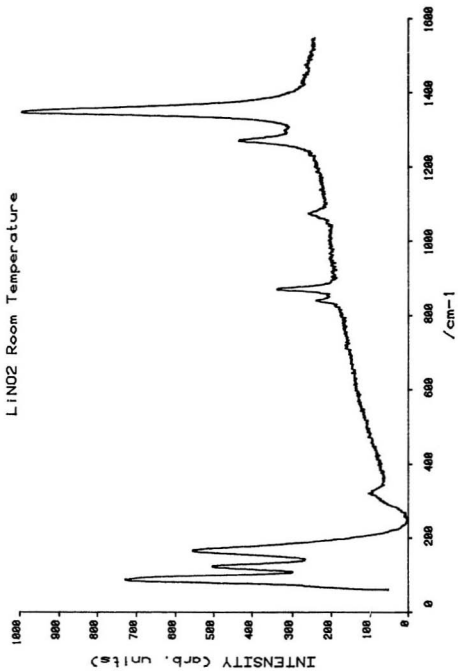


Figure 7. Raman spectrum of LiNO_2 sealed under $\text{NO}(\text{g})$ recorded at room temperature using the blue 4880 \AA line. $\nu_{\text{initial}} = 60 \text{ cm}^{-1}$.






Figure 8. Raman spectrum of LiNO_2 sealed under $\text{NO}(\text{g})$ recorded at 471 K using the blue 4880 Å line. $\nu_{\text{initial}} = 60 \text{ cm}^{-1}$. There is no evidence for a high temperature phase. Peaks in the low frequency region are thermally expanded lattice modes of the low temperature phase.

LINO2 @ 471K

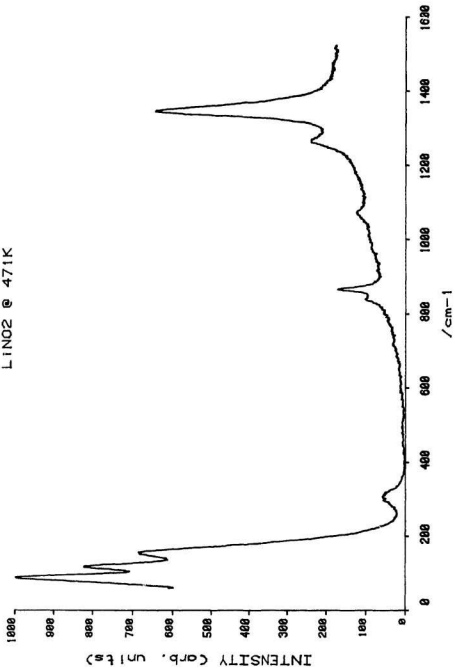


Figure 9. Intensity, $I(\omega)$, Raman spectra of LiNO_2 melt under $\text{NO}(\text{g})$ recorded at 505 K using the blue 4880 Å line. $\nu_{\text{initial}} = 60 \text{ cm}^{-1}$.

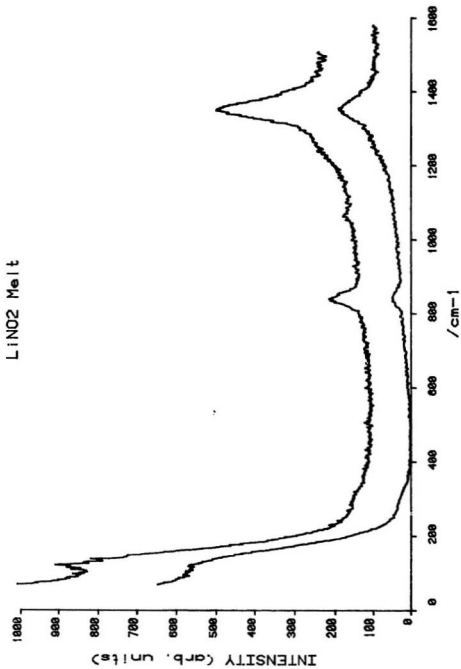


Figure 10. Reduced, $R(\omega)$, Raman spectra of LiNO_2 melt under $\text{NO}(\text{g})$ recorded at 505 K using the blue 4880 Å line. $\nu_{\text{initial}} = 60 \text{ cm}^{-1}$.

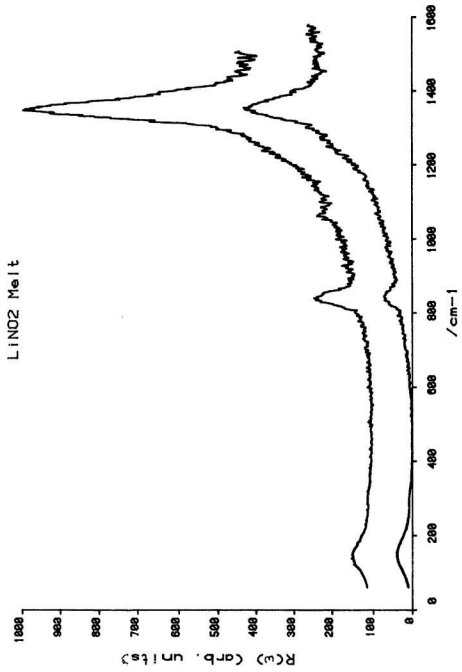
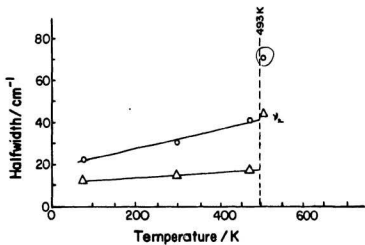
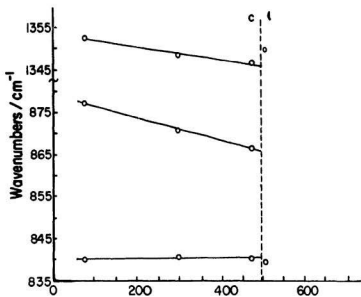


Table 3. Peak Frequencies and Halfwidths for Lithium Nitrite at Various Temperatures s = strong, w = weak, m = medium, sp = sharp, br = broad.

TEMPERATURE					
Frequency/cm ⁻¹		(Halfwidth/cm ⁻¹)			Assignment
77 K c	298 K c	471 K c	505 K l		
66.5 w				ν_L	
84.5 (s,sp)	88.0 (s,sp)	89.0 (s,sp)		ν_L	
97.0 (s,sp)				ν_L	
130.0 (s,sp)	123.5 (s,sp)	118.5 (s,sp)	137.5 (w,br)	ν_L	
160.0 (sh)	166.0 (s,sp)	155.0 (s,sp)		ν_L	
173.0 (s,sp)				ν_L	
194.0 (sh)	320.5 (w,br)	307.0 (w,br)		ν_L	
840.0 (12.2)	840.5 (14.9)	840.5 (17.6)	839.5 (41.4)	ν_2	
877.0 (12.2)	870.5 (14.9)	866.5 (17.6)			
-	1075.0	1073.0	1064.0	$\nu_1(\text{NO}_2^-)$	
1276.0	1271.5	1266.5	-	ν_3	
1352.5 (22.4)	1348.5 (30.5)	1347.0 (40.7)	1350.0 (71.2)	ν_1	

Note: ν_L = lattice mode

Figure 11. Temperature dependence of ν_1 and ν_2 frequencies and halfwidths for LiNO_2 .



is in agreement with the spectroscopic studies of Carr et al (1979).¹⁹

The spectra of ordered LiNO_2 solid show a splitting of the ν_2 bending mode of the nitrite ion with bands at 840 cm^{-1} and about 870 cm^{-1} . This splitting is believed to be too large to be due to correlation field splitting (Brooker and Irish, 1971)²⁰ and is attributed to the presence of two distinct nitrite sites in the crystal. The low frequency component of ν_2 corresponds to the lithium cation interacting with the nitrite ion through the nitrogen (nitro linkage), whereas the high frequency component corresponds to interaction through the oxygen atoms (nitrito linkage). Since the intensity of the 870 cm^{-1} band is approximately twice that of the 840 cm^{-1} band, the more occupied site for the NO_2 is that with nitrito linkage.

Optimized geometries obtained for nitro and nitrito LiNO_2 by ab initio calculations also indicate that the nitrito linkage is energetically more favorable. Details of the ab initio study are presented as Appendix 1.

Lithium nitrite is ordered therefore the suggested symmetry group, D_{3d}^5 is not possible since it would place the NO_2 group on a site symmetry greater than for the free ion. The site symmetry for an ion or molecule in a crystal is generally less than that for the free ion or molecule. The external lattice modes are similar to those for the sodium salt which suggests LiNO_2 may also belong to a C_{2v} space group. However, LiNO_2 unlike the other alkali metal nitrites has a split ν_2 mode, suggesting two stable sites for the nitrite group as previously discussed.

LiNO_2 melt did decompose slowly but decomposition was suppressed by sealing the sample under $\text{NO}(\text{g})$. The spectra of molten LiNO_2 (figures 9,10) are quite different than the high-temperature spectrum (figure 8). The lattice mode in the melt is very broad and is hidden in the Rayleigh wing which is indicative of the relatively free nitrite ion. In addition, the ν_2 band is a broad singlet, centered about 840 cm^{-1} . Melting was accompanied by abrupt changes in the internal mode peak positions and halfwidths (figure 11). While ν_1 and ν_2 frequencies both decreased on

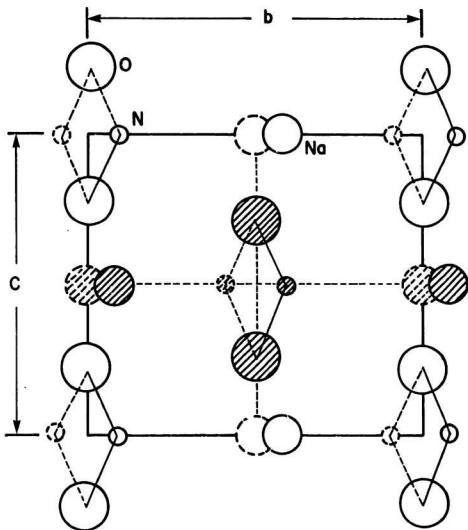
heating, ν_1 increased drastically on melting whereas ν_2 decreased drastically. These results are in conflict with those reported by Prisyazhni (1976)²¹ who observed an increase in ν_1 frequency on heating. Note that the low-frequency peak of ν_2 appears to be temperature independent; even upon melting this peak only shifted 0.5 cm^{-1} to a lower wavenumber, whereas the high-frequency component disappeared upon melting. The halfwidths slowly increased with heating, but upon melting there was a sudden increase. These spectral changes in peak positions and halfwidths are characteristic of a phase transition from an ordered to a disordered arrangement of nitrite ions upon melting.

NaNO₂

Ferroelectric sodium nitrite is ordered and has space group symmetry C_{2v}^{20} with a single NaNO₂ molecule per unit cell (Zeigler, 1931).⁵ The molecule lies in the crystallographic bc plane with the NO₂⁻ ions aligned such that the dipole moments all point in the same direction and parallel to the b axis. The order-disorder transition actually occurs in two steps^{3b}. First at about 436 K, the Curie temperature, a transition to an antiferroelectric, or ferroelectric, phase occurs. Here, the sinusoidal modulation of the average dipole moment appears in the a direction. Second, at about 437 K, the Neel temperature, a transition from this ferroelectric phase to a paraelectric phase occurs. In the paraelectric phase, the crystal is disordered and the nitrite ions point in either direction along the b axis. X-ray analysis has determined this phase to have D_{2h}^{25} space group symmetry with an ac mirror plane (Strijk and Macbillavry, 1946).⁶ (Figure 12) Therefore the nitrogen atom exists on two lattice sites in the disordered phase. Although the order-disorder transition occurs in two steps, it is the overall, combined transition that is most often considered.

There is much debate concerning the mechanism of the orientational disordering of the nitrite ions; three possible processes exist: (1) the in-plane rotation of the NO₂⁻

Figure 12. Unit-cell of NaNO_2 , ferroelectric, C_{2v}^{20} point group symmetry. Dashed circles represent the paraelectric phase, D_{2h}^{25} , where nitrite is on two distinct sites.



ions around the *a* axis, (2) the out-of-plane rotation of the NO_2^- ions around the *c* axis, or (3) the tunneling of the N atoms through the potential barrier between the two equilibrium configurations. Sato et al (1961)²⁸ studied the phase transition in NaNO_2 polarized infrared radiation and ruled out the third possibility, therefore the transition involves an in-plane rotation about the *a* axis or an out-of-plane rotation about the *c* axis, or some combination of the two.

Spectroscopic studies by several workers (Brehat and Wyncke, 1985²³; Jurneau, 1981²⁴; Goncharuk and Chisler, 1976²⁵; Ivanova and Chisler, 1976²⁶; Hartwig et al, 1972^{13b}; Chisler and Shur, 1966²⁷; Sato et al, 1961²⁸; and Andrade et al, 1973⁶²) indicated that the transition was more probably realized by rotation about the *a* axis. Optical measurements by Dio and Yanagi (1973)²⁹, Vogt and Happ (1971)³⁰ and Ota et al (1970)³¹ support this thesis. On the other hand, theoretical calculations by Ehrhardt and Michel (1981)³² based on atomic sterical hindrance potentials, molecular dynamic calculations by Lynden-Bell et al (1986)³³ and Klein and MacDonald (1982)³⁴; neutron diffraction studies by Kay et al (1975)³⁵, Nümura and Muto (1973)³⁶, and Shibuya et al (1970)³⁷; x-ray studies by Suzuki et al (1981, 1971)³⁸ and Shibuya et al (1970)³⁷; and a ^{23}Na nmr study by Betsuyaku (1969)³⁹ all indicated a rotation about the *c* axis was more probable.

Raman spectra obtained for sodium nitrite from 77 K to the melting point, 551 K and of the melt are represented in figures 13 to 23. The study includes spectra showing the temperature dependence of an oriented single crystal. Table 4 gives the peak frequencies for various phases of NaNO_2 , and Table 5 presents the frequencies and halfwidths for the ν_1 and ν_2 modes at all temperatures used over the range investigated.

The low-temperature spectrum (figure 13) of powdered NaNO_2 contains eight distinct peaks, consistent with an ordered solid of space group C_{2V}^{20} with Raman active modes $3A_1 + 3B_1 + A_2 + 2B_2$. One A_1 lattice mode at 194 cm^{-1} appears too

Figure 13. Raman spectrum of NaNO_2 powder which was never melted, recorded at 77 K using the blue 4880 Å line. $\nu_{\text{initial}} = 31 \text{ cm}^{-1}$. The NaNO_2 , III, is in an ordered ferroelectric phase.

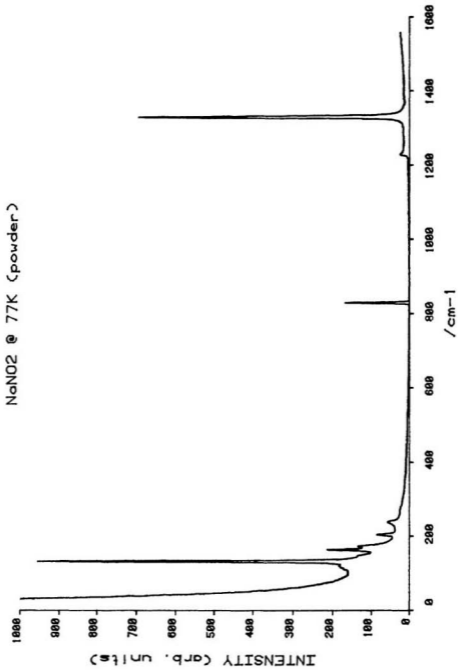


Figure 14. Raman spectrum of a NaNO_2 single crystal recorded at 298 K using the blue 4880 Å line. $\nu_{\text{initial}} = 20 \text{ cm}^{-1}$. This is the "regular" orientation with ν_3 at 1228 cm^{-1} . The B_1 (TO) modes are allowed but there is some spill-over of the A_1 (TO) modes (827 and 1324 cm^{-1}) and the A_2 mode (119 cm^{-1}). The phase is ferroelectric.

NaNO2 @ 298K (Single Crystal)

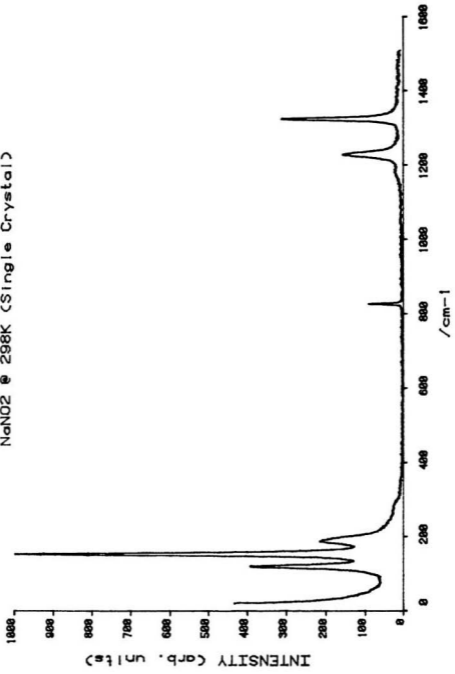


Figure 15. Intensity, $I(\omega)$, Raman spectra of NaNO_2 melt recorded at 573 K using the green 5145 Å line. $\nu_{\text{initial}} = 44 \text{ cm}^{-1}$.

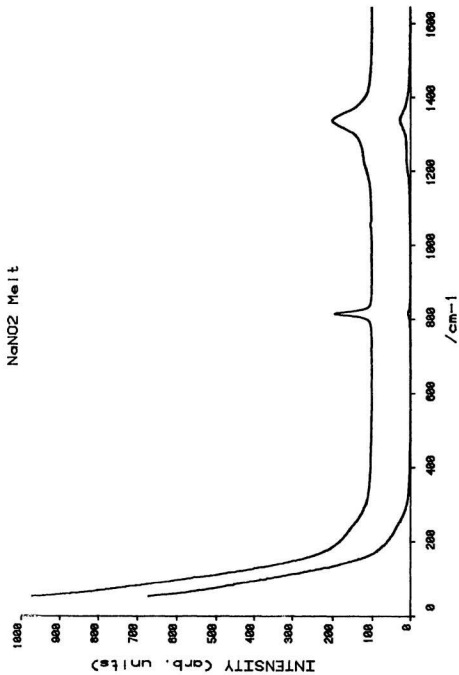


Figure 16. Reduced, $R(\omega)$, Raman spectra of NaNO_2 melt recorded at 573 K using the green 5145 Å line. $\nu_{\text{initial}} = 44 \text{ cm}^{-1}$.

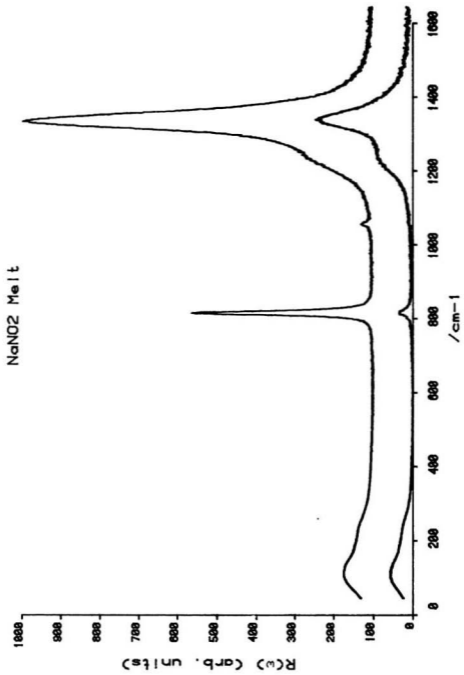


Figure 17. Raman spectrum of paraelectric, disordered NaNO_2 I recorded at 530 K using the blue 4880 Å line. $\nu_{\text{initial}} = 50 \text{ cm}^{-1}$.

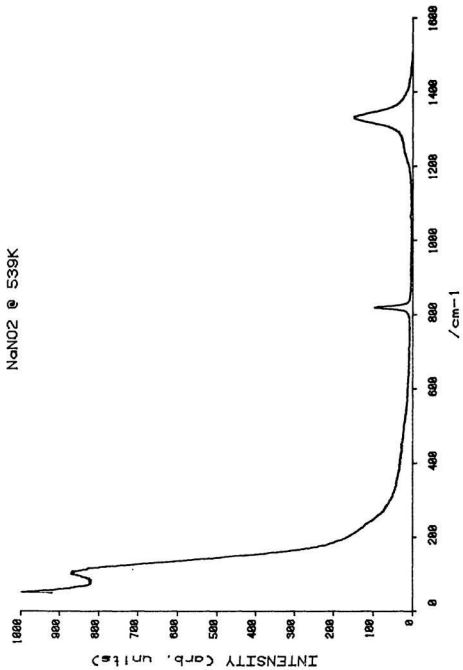


Figure 18. Raman spectrum of a NaNO_2 oriented single crystal recorded at 77 K using the blue 4880 Å line. $\nu_{\text{initial}} = 20 \text{ cm}^{-1}$. The ν_3 LO mode is positioned at 1358.5 cm^{-1} , shifted $\sim 128 \text{ cm}^{-1}$ from its "regular" frequency. The crystal orientation is $y(xz)x$ where x and y are 110 planes.

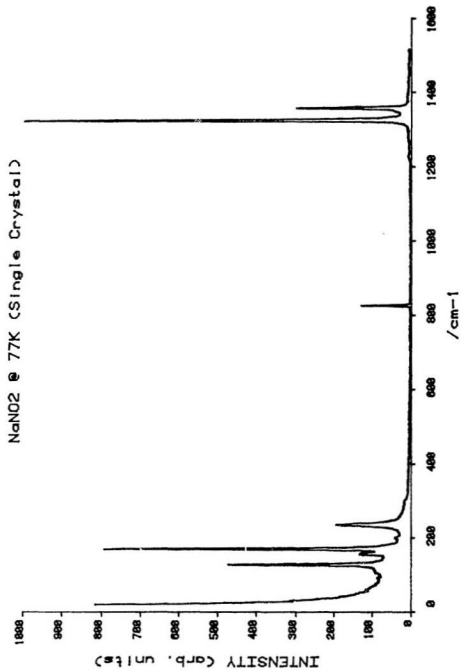


Figure 19. Raman spectrum of a NaNO_2 oriented single crystal recorded at 208 K using the blue 4880 Å line. $\nu_{\text{initial}} = 30 \text{ cm}^{-1}$. The ν_3 LO mode has shifted $\sim 128 \text{ cm}^{-1}$ from its "regular" frequency. Also, the ν_3 mode is approximately two times as intense as the ν_1 mode. Crystal orientation is $y(xz)x$ where x and y are 110 planes.

NaN02 Oriented Crystal @ 298K

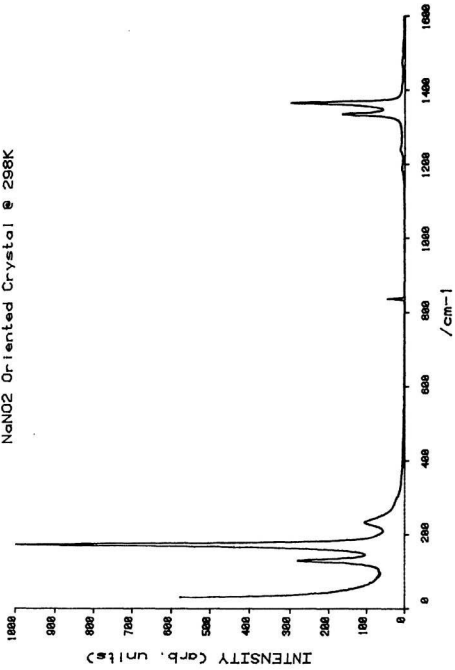


Figure 20. Intensity, $I(\omega)$, Raman spectra of the ν_1 , ν_3 region of NaNO_2 oriented single crystal as it went through the order-disorder phase transition. Spectra were recorded using the blue 4830 angstrom line at: A) 298 K; B) 383 K; C) 413 K; D) 434 K; and E) 458 K. $\nu_{\text{initial}} = 30 \text{ cm}^{-1}$. ν_3 shifted $\sim 105 \text{ cm}^{-1}$. Crystal orientation is $y(xz)x$ where x and y are 110 planes.

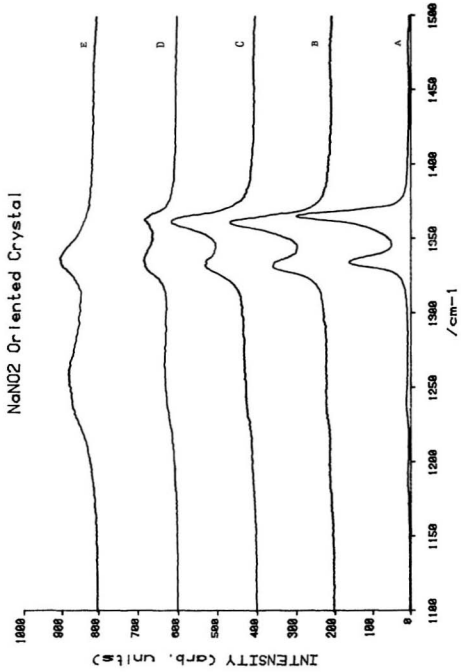


Figure 21. Raman spectrum of NaNO_2 oriented single crystal at 434 K recorded using the blue 4880 Å line. $\nu_{\text{initial}} = 30 \text{ cm}^{-1}$. The ν_3 mode appears at its "regular" and "oriented" frequencies as it neared the 436 K phase transition. Crystal orientation is $y(xz)x$ where x and y are 110 planes.

NaNO₂ Oriented Crystal @ 434K

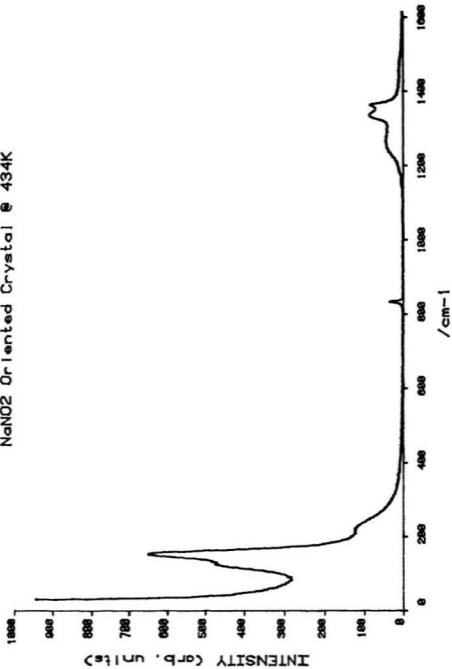


Figure 22. Raman spectrum of the NaNO_2 oriented single crystal as portrayed in Figures 17-20 recorded at 458 K using the blue 4880 Å line. $\nu_{\text{initial}} = 30 \text{ cm}^{-1}$. The ν_3 TO mode is positioned at 1250 cm^{-1} in the paraelectric, disordered phase.

NaNO₂ Oriented Crystal @ 458K

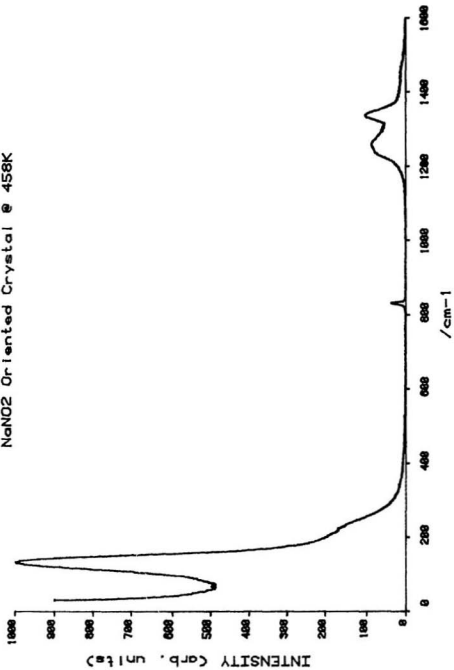


Figure 23. Reduced, $R(\omega)$, Raman spectra of the low frequency region of NaNO_2 oriented single crystal as it went through the order/disorder phase transition. Spectra were recorded using the blue \AA line at: A) 298 K; B) 383 K; C) 413 K; D) 434 K; and E) 458 K. $\nu_{\text{initial}} = 30 \text{ cm}^{-1}$. Crystal orientation is $y(xz)x$ where x and y are 110 planes.

NaNO₂ Oriented Crystal

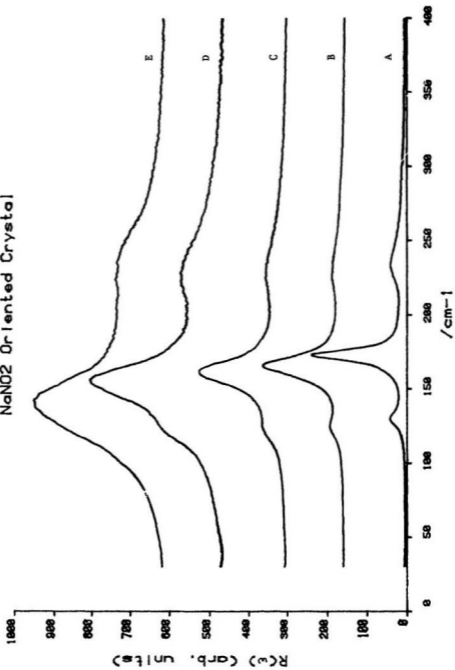


Table 4. Peak Frequencies (in cm^{-1}) for TO Modes for the Different Phases of Sodium Nitrite.

77 K III	298 K III	539 K I	573 K I	Assignment ^a
133.5 (vs,sp)	119.5 (s,sp)	104.5 (s,br)	112.0 (2,br)	$\nu_L(A_2, R_b)$
164.5 (s,sp)	150 (m,sp)			$\nu_L(B_2, T_a)$
173.5 (m,sp)	153.5 (vs,sp)			$\nu_L(B_1, R_a)$
205.5 (m,sp)	187.0 (s,sp)			$\nu_L(B_1, T_c)$
	195 ^b			$\nu_L(A_1, T_b)$
239.0 (m,sp)	228 (m,sh)	~ 215	~ 250 (br)	$\nu_L(B_2, R_c)$
830.5 (s,sp)	826.5 (m,sp)	820.0 (m,sp)	816.0 (w,sp)	$\nu_2(A_1)$
1230.5 (w,sp)	1228.0 (m,sp)	- (sh)	- (sh)	$\nu_3(B_1)$ TO
1331.0 (vs,sp)	1324.0 (s,sp)	1332.5 (s,br)	1338.0 (m,br)	$\nu_1(A_1)$

a based on Ref. 13b.

b infrared value (Ref. 13b), although Raman allow this mode is too weak to observe.

Table 5. Peak Frequencies and Halfwidths of ν_1 and ν_2 for Sodium Nitrite* at Various Temperatures.

Temperature/K	ν_1	ν_2
	frequency (halfwidth)/cm ⁻¹	frequency (halfwidth)/cm ⁻¹
77	1327.5 (6.4)	829.0 (7.14)
298	1324.0 (11.5)	826.5 (7.14)
383	1322.0 (15.8)	825.0 (7.14)
413	1322.0 (18.6)	824.5 (7.14)
434	1326.0 (30.1)	823.5 (7.14)
458	1327.0 (42.0)	821.5 (8.93)
539	1331.0 (42.5)	820.0 (10.31)
573	1338.0 (64.3)	816.0 (14.28)

* Oriented single crystal.

weak to be observed in the Raman but it has been observed in the infrared^{13b}. A correlation of these modes to the observed peaks is illustrated in Table 6. The room temperature spectrum (figure 14) is also consistent with this structure, although the lattice modes are slightly broader. These results are in excellent agreement with previously reported spectra of NaNO_2 . There was no evidence for a possible phase transition at 178 K reported by Gesi (1969)⁶³; the temperature dependence plots of ν_1 and ν_2 positions and halfwidths showed no discontinuous changes prior to the order-disorder phase transition at about 436 K (figure 24).

The frequencies of ν_1 and ν_2 both decreased gradually from 77 K to 436 K at which point ν_1 shifted to a higher wavenumber whereas ν_2 suddenly shifted to a lower wavenumber. ν_2 continued to decrease to the melting point where it showed another sudden decrease, but ν_1 increased steadily to the melting point and then shifted to an even higher wavenumber. The halfwidths of ν_1 and ν_2 also showed discontinuous changes at the phase transitions, increasing from 77 K to the melt. Von der Lieth and Eysel (1982)⁶⁴, based on their Raman study of NaNO_2 , report an unusually marked change of shape and maximum position with temperature for both ν_1 and ν_2 . Each band consists of two components caused by 'multiple site' splitting due to orientational disorder, but they are not well resolved into separate peaks because of the bandwidths. Both ν_1 and ν_2 become more and more asymmetric with increasing temperature as Γ increases until well above the phase transition when Γ and Γ^+ are approximately equal. Γ is the intensity of the component due to nitrite ions oriented with their molecular dipole oriented towards the -b crystallographic direction, and Γ^+ is the intensity of the component due to nitrite ions pointing towards +b. The results of Von der Lieth and Eysel⁶⁴ and Hartwig et al^{13b} indicate that the disordered form_A[±] of NO_2^- are present even at room temperature and that the relative number of disordered NO_2^- increases with increased temperature until at the phase transition the random disorder is achieved suddenly. This interpretation is

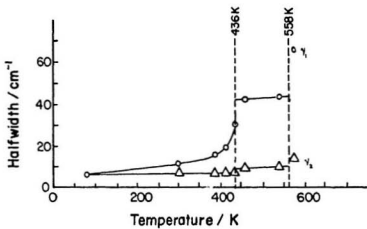
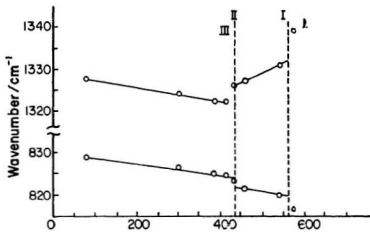
Table 6. Assignment of Normal Modes of Vibration in NaNO_2 ^a

Frequency		Intensity ^b		Assignments
TO	LO	Raman	Infrared	
120	-	vs	ia	A_2, α_{ac} rotation about b
150	201	m	vs	B_2, T_a, α_{ab} trans a
154	165	s	m	B_1, T_c, α_{bc} rotation about a
185	236	ms	vs	B_1, T_c, α_{bc} rotation trans c
194	269	-	vs	$A_1, T_b, \alpha_{aa}, \alpha_{bb}, \alpha_{cc},$ trans b
228	254	vs	m	B_2, T_a, α_{ab} rotation about c
827.5	829	s	m	$\nu_2 A_1$ symmetric bend
1225	1356	m	vs	$\nu_3 B_1$ antisymmetric stretch
1326	1328	vs	vw	$\nu_1 A_1$ symmetric stretch

a Based on the work of Porto et al, Ref. 13b.

b vs, very strong; m, medium; vw, very weak; ia, inactive

Figure 24. Temperature dependence of ν_1 and ν_2 frequencies and halfwidths for NaNO_2 .



supported by the thermal study^{13a} of the phase transition which showed that the anomalous rise in heat capacity increased gradually from 100 °C to the transition temperature.

The different crystal structure of the high-temperature, paraelectric phase of NaNO_2 can be seen in the spectrum recorded at 539 K; the external lattice mode region is now represented by a broad band with a shoulder and ν_3 is a shoulder of ν_1 which is much broader. These characteristics are consistent with partially a disordered solid.

Paraelectric NaNO_2 has been assigned to D_{2h}^{25} crystallographic symmetry and normal modes of vibration for this crystal have been predicted (Iqbal and Owens⁶⁵, and Hartwig^{13b}). However these predictions are not in agreement with the observed vibrational spectrum. A density of states is observed in a vibrational spectrum and broad bands, particularly in the low frequency region are observed for disordered solids. While a spectrum gives an average frequency of all the vibrational modes for an immediate sample symmetry over the vibrational period, (picosecond) a unit-cell analysis such as X-ray assumes the long time averaged symmetry of the entire crystal. As such, a true symmetry of a disordered solid is not obtained by crystallographic studies like X-ray. X-ray analysis predict disordered NaNO_2 crystals have D_{2h} symmetry which is higher than the symmetry for the free molecule. This is not possible since a molecule is generally distorted to a lower symmetry in the solid state. Hartwig et al recognize this fact in their paper and explain the "misuse of the X-ray determined crystalline symmetry to describe the Raman scattering".^{13b}

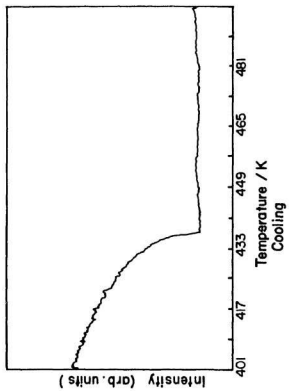
The Raman spectra of molten NaNO_2 (figures 15,16) is similar to the high-temperature spectrum (figure 17), confirming the orientational disorder of the nitrite ions in paraelectric NaNO_2 . Little change is noted between these spectra since much of the disorder has already occurred at 436 K.

The anti-symmetric stretching ν_3 mode of NaNO_2 has a longitudinal optic (LO) mode, that is it has an electric vector parallel to the propagation direction. The exact energy or frequency of LO modes for this crystal structure depends on the propagation direction of the exciting wave, hence LO modes show a pronounced orientational dependence for non-centric crystals with low symmetry such as ferroelectric NaNO_2 . Spectra were obtained at various temperatures for a single crystal oriented such that the LO mode had shifted to a higher frequency (ie. $y(xz)x$ where y and x are 110 planes. $y(xz)x$ could also be written as $110(110, 001)110$). Figures 18 and 19 show spectra at 77 K and 298 K respectively; here the LO mode has shifted to 1358.5 cm^{-1} and 1355.5 cm^{-1} respectively. The non-oriented crystal shows TO modes at 1230.5 cm^{-1} and 1228 cm^{-1} for 77 K and 298 K respectively.

The oriented crystal was heated and Raman spectra recorded at various temperatures through the reported 436 K order-disorder phase transition to 458 K. As the crystal underwent this phase transition to a disordered centro-symmetric solid, space group D_{2h}^{25} , the LO mode at 1355 cm^{-1} began to disappear, (figure 25) while the TO ν_3 mode at 1230 cm^{-1} reappeared (figure 20). A spectrum recorded at 434 K shows the presence of the LO mode at 1353 cm^{-1} and the TO mode at 1255 cm^{-1} (figure 21). At 458 K the primary ν_3 band is centered at about 1250 cm^{-1} while a very weak signal remains at higher frequency (figure 22). The disappearance of the LO mode provided a good method for studying this phase transition.

The external modes were also carefully studied through the phase transition, particularly A_2 , B_1 and B_2 which correspond to rotations about the b , a and c axes respectively (figure 23). A_2 occurs at the lowest frequency, $\sim 120 \text{ cm}^{-1}$, therefore rotation about b is least hindered. But, this is not surprising since such a motion doesn't change the basic symmetry of the crystal - the nitrite ions maintain their orientation along the b axis. However, the relative frequencies of the B_1 and B_2 modes are of greater concern since one of these modes is believed to be the key to

Figure 25. Intensity of LO mode for NaNO_2 recorded at 1355 cm^{-1} using the blue 4880\AA line. The sample was cooling.



the mechanism for the order-disorder transition. B_1 has a frequency of about 163 cm^{-1} whereas B_2 has a frequency of about 224 cm^{-1} . The molecular dynamics calculations of Lynden-Bell et al (1986)³³ have confirmed these assignments. Therefore, rotation about the a axis is more facile than rotation about the c axis. The greatest change observed through the phase transition was in the B_1 which shifted about 30 cm^{-1} to a lower wavenumber. B_2 , on the other hand, only shifted about 10 cm^{-1} to a lower frequency (figure 23). The large decrease in B_1 frequency with increase in temperature especially near the phase change, indicates the potential barrier to rotation about the a axis is relaxed enough to lead to the orientational disorder of the nitrite ions. These spectroscopic results are in complete agreement with those of previous workers (Hartwig et al, 1972^{13b}; Brehat and Wyncke, 1985²³; Sato et al, 1961²⁸; Chisler and Shur, 1966²⁷; Dyanova and Chisler, 1976²⁶; Goncharuk and Chisler, 1976²⁵; and Jumeau, 1981²⁴). Barnoski and Ballantyne (1968)⁵⁶ have concluded based on a Kramers-Kronig analysis of the temperature dependence reflection spectrum that the mechanism involves rotation about the c axis. However, these authors have either mislabelled the a and c axes or have misassigned the 220 cm^{-1} and 154 cm^{-1} (B_2 and B_1) peaks, hence, their results also indicate a mechanism involving a rotation about the a axis. The ultrasonic velocity measurements by Ota et al (1970)³¹ indicated the packing of atoms is the most dense along the a direction and atoms or ions in any one bc plane may feel the strongest repulsion when displaced in the a direction. This too is evidence in support of an a axis rotation.

The spectroscopic results do not agree with molecular dynamics calculations of Lynden-Bell, et al (1988)³³ and Ehrhardt and Michel (1981)³². However, the M.D. calculations do not consider the important electronic effects but assume point charges. The topographic study by Suzuki and Takagi (1971)³⁸ also supports the M.D. calculations. However this domain walls study, like the M.D. calculations neglects the electrons around N. The model therefore requires unrealistic charges on

N and O ($N = 2.64$ and $O = -1.82$). Ab initio calculations (details of which are given in Appendix I) do account for electronic effects. The consideration of electronic charges gives a more accurate account since the transition does involve a polarizability change. The ab initio study supports the theory of an a axis rotation.

The ab initio study (Appendix I) indicates that the NO_2^- ion is best represented by an oblate spheroid with an almost even charge distribution about the plane. In this regard the charge distribution of NO_2^- resembles that of NO_3^- because of the excess non-bonded electronic charge at the N of NO_2^- . It is well known that the disordered phases of alkali metal nitrate salts are achieved through reorientation about the axis perpendicular to the plane (i.e., a axis rotation) and a similar mechanism would be reasonable for nitrite. Furthermore there is no dispute over the fact that the NO_2^- remains in the bc plane in each of the three phases which also suggests that the a axis rotation is not unreasonable.

KNO_3

Crystallographic data for the standard pressure polymorphs of KNO_3 is summarized in Table I. The high-temperature phase, I, changes to a room temperature phase, II, at about 313 K (Ray, 1960⁹; Parry et al, 1964⁶⁷; and Mraw et al, 1978¹⁴), and further transition to a low-temperature phase, III, occurs at about 260 K (Ray, 1960⁹; Solbakk and Stromme, 1969⁸; and Mraw et al, 1978¹⁴). Richter and Pistorius (1972)⁷ using x-ray analysis found another transition at about 230 K to a lower temperature monoclinic phase, VII, however Mraw et al (1978)¹⁴ did not observe this transition in their calorimetric investigations. The transition was observed in the recent Raman spectroscopic study by Adams et al (1988)⁴⁰. Tanisaki and Ishimatsu (1965)⁴² reported a further transition at 343 K based on x-ray data, and in support of this, Tse et al (1986)⁴³ reported spectroscopic evidence for a transition at about 380 K.

Figure 26. Raman spectrum of KNO_2 III recorded at 77 K using the blue 4880 Å line. $\nu_{\text{initial}} = 20 \text{ cm}^{-1}$. This is an ordered phase.

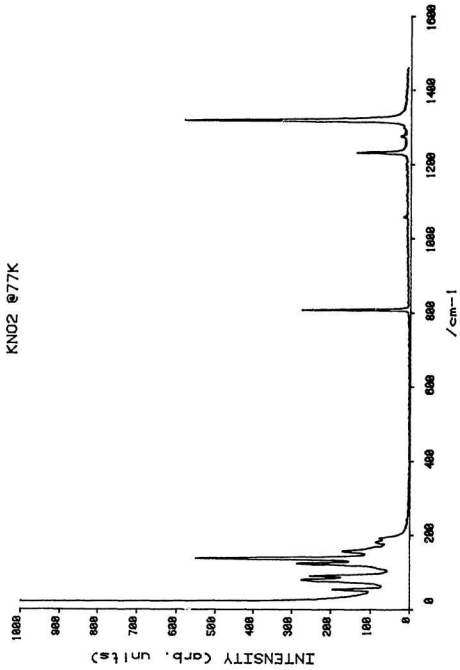


Figure 27. Raman spectra of KNO_2 as it went through the III/II, order-disorder phase transition at 264 K. The spectra were recorded using the blue 4880 Å line at: A) 102 K; B) 127 K; C) 152 K; D) 177 K; E) 202 K; F) 227 K; G) 252 K; and H) 273 K. $\nu_{\text{initial}} = 20 \text{ cm}^{-1}$.

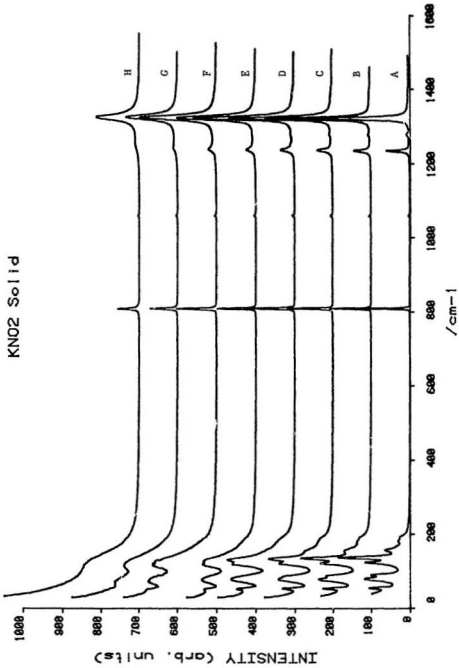


Figure 28. Raman spectra of the low frequency region of KNO_2 as it went through the III/II order-disorder phase transition. Spectra were recorded using the blue 4880 \AA line at: A) 77 K; B) 152 K; C) 202 K; D) 252 K; and E) 273 K.

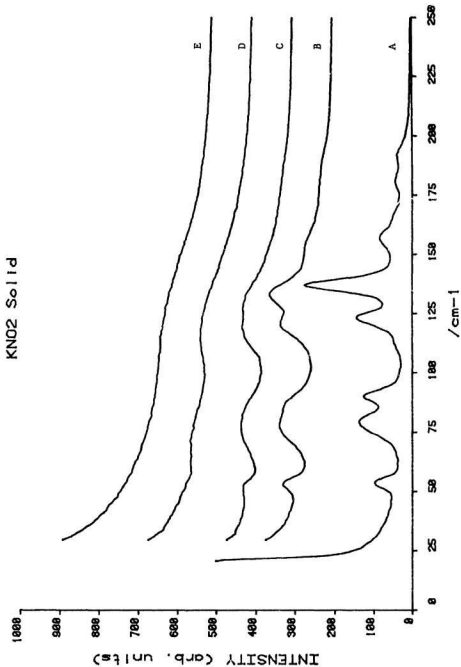


Figure 29. Raman spectra of KNO_2 II recorded at 298 K using the blue 4880 Å line.
 $\nu_{\text{initial}} = 87.0 \text{ cm}^{-1}$. This is the disordered phase.

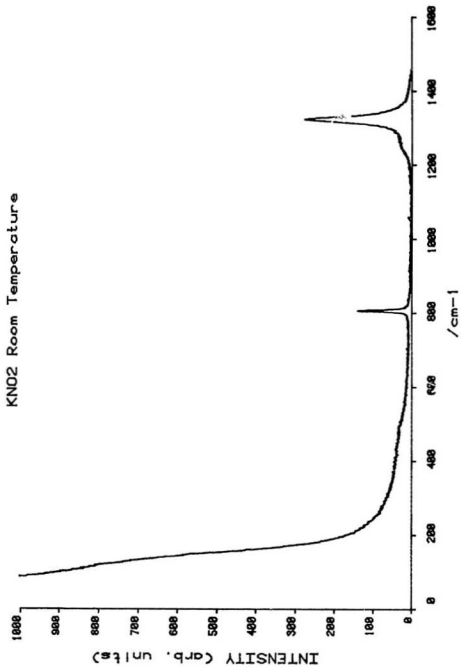


Figure 30. Raman spectrum of KNO_2 I at 630 K, in the reported high temperature phase. The spectrum is simply that of the room temperature phase (II). Spectrum was recorded using the 4880 Å line. $\nu_{\text{initial}} = 50 \text{ cm}^{-1}$.

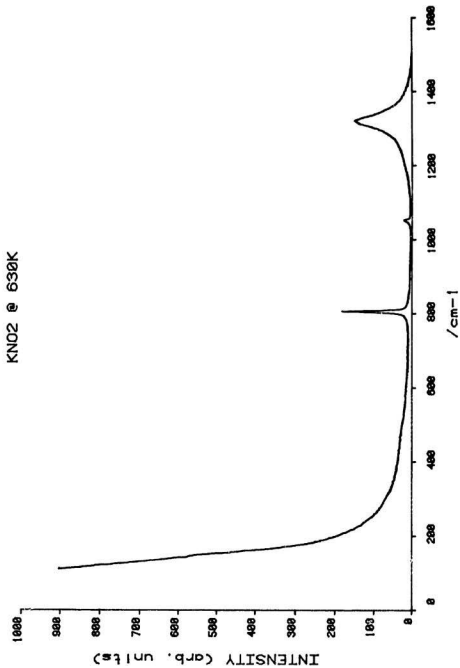


Figure 31. Intensity, $I(\omega)$, Raman spectra of KNO_2 melt recorded at 703 K using the blue 4880 Å line. $\nu_{\text{initial}} = 30 \text{ cm}^{-1}$.

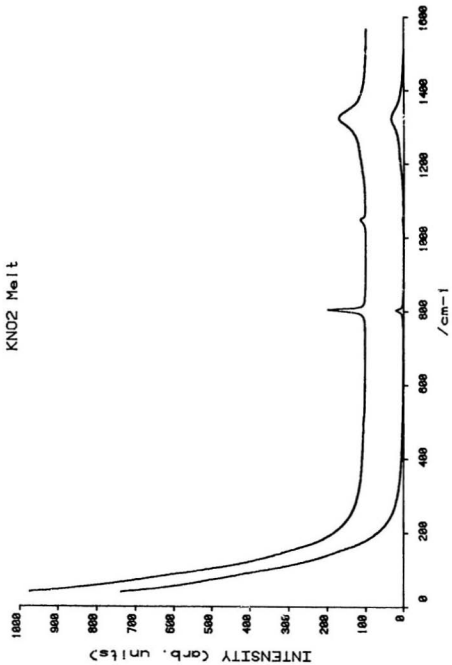
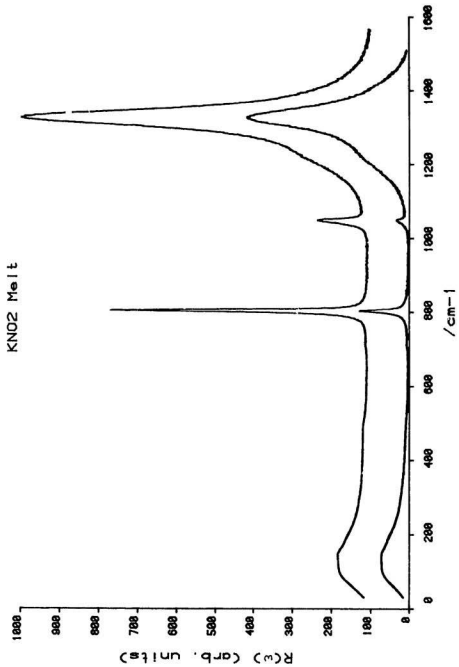


Figure 32. Reduced, $R(\omega)$, Raman spectra of KNO_2 melt recorded at 703 K using the blue 4880 Å line. $\nu_{\text{initial}} = 30 \text{ cm}^{-1}$.



The high-temperature and room-temperature phases, I and II, of KNO_2 are disordered (Solbakk and Stromme, 1969)⁸ whereas the two low temperature phases, III and VII are said to be ordered. The enthalpy and entropy of transition for both the III/II and II/I transitions were determined by Mraw et al (1978)¹⁴ (Table 2). As expected, the energy required for the III/II order-disorder transition is greater than that required for the II/I disorder-disorder transition.

In addition to the detailed Raman spectroscopic work of Adams et al (1988)⁴⁰, a few other spectroscopic investigations of KNO_2 have been reported. Brooker and Irish(1971)²⁰ recorded a Raman spectrum of KNO_2 II at room-temperature, Carr et al (1970)¹⁹ recorded a spectrum of KNO_2 VII at 18 K, Tse et al (1986)⁴³ recorded spectra over the 300-400 K temperature range and Prisyazhnyi et al (1976)²¹ obtained a spectrum of the melt.

Raman spectra of potassium nitrite obtained over the temperature range 77 K to the melting point, 665 K, and for the melt are illustrated in figures 26 to 32. Four different solid phases were observed. Table 7 gives the peak frequencies of the Raman spectra for the four solid phases and the melt, and Table 8 gives the frequencies and halfwidths for the ν_1 and ν_2 modes at all temperatures used over the range investigated.

The spectrum of phase VII recorded at 77 K (figure 26) is typical of an ordered solid; there are several well defined lattice modes in addition to the three sharp internal modes. This spectrum is in excellent agreement with that observed by Carr et al (1970)¹⁹ at 18 K except the peak at 42 cm^{-1} is lost in the Rayleigh line. The progress of the Raman spectrum upon heating to room temperature is presented in figure 27. Figure 33 displays the changes in ν_1 and ν_2 frequencies and halfwidths with temperature. The ν_2 frequency remained constant on heating to 177 K at which point it decreased linearly to 252 K through the VII/III transition. It then shifted down sharply 1.5 cm^{-1} at the II/II transition and remained constant to the

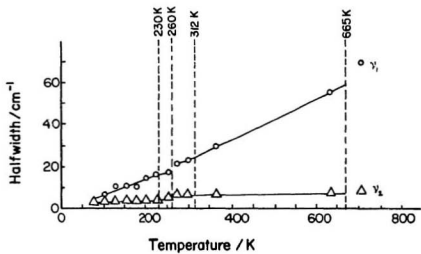
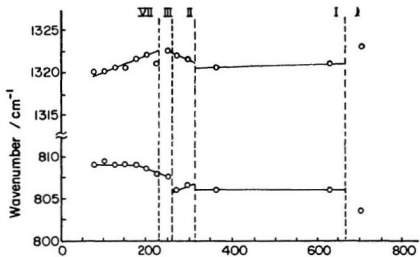
Table 7. Peak Frequencies (in cm^{-1}) for the Different Phases of Potassium Nitrite.

77 K VII	252 K III	298 K II	630 K I	703 K I	Assignment
53.5 (m,sp)	44 (sh)				ν_L
79.5 (s,sp)	72.5 (w,br)	-	-	139.5 (w,br)	ν_L
90.0 (s,sp)	119 (w,br)				ν_L
123.5 (s,sp)					ν_L
137.5 (vs,sp)					ν_L
157.0 (m,sp)					ν_L
179.5 (w,sp)					ν_L
192.0 (w,sp)					ν_L
809.0 (s,sp)	807.5	806.5 (m,sp)	806.0 (m,sp)	803.5 (m,sp)	ν_2
1056 (vw)	1056 (vw)	1056 (vw)	1052 (vw)	1048 (vw)	$\nu_1(\text{NO}_2^-)$
1232.0 (m,sp)		1256 (sh)	-	-	ν_3
1320.0 (vs,sp)	1322.5	1321.5 (s,sp)	1321.0 (m,br)	1323.0 (m,br)	ν_1

Table 8. Peak Frequencies and Halfwidths of ν_1 and ν_2 for Potassium Nitrite at Various Temperatures.

Temperature/K	ν_1 frequency (halfwidth)/cm ⁻¹	ν_2 frequency (halfwidth)/cm ⁻¹
77	1320.0 (3.5)	809.0 (3.5)
102	1320.0 (6.9)	809.5 (3.5)
127	1320.5 (10.3)	809.0 (3.5)
152	1320.5 (10.3)	809.0 (3.5)
177	1321.5 (10.3)	809.0 (3.5)
202	1322.0 (13.8)	809.5 (3.5)
227	1321.0 (15.9)	808.0 (3.5)
252	1322.5 (17.2)	807.5 (5.5)
273	1322.0 (21.3)	806.0 (6.2)
298	1321.5 (22.7)	806.5 (6.2)
365	1320.5 (29.5)	806.0 (6.2)
630	1321.0 (55.0)	806.0 (6.9)
703	1323.0 (69.0)	803.5 (8.3)

Figure 33. Temperature dependence of ν_1 and ν_2 frequencies and halfwidths for KNO_2 .



melting point where it shifted a further 2.5 cm^{-1} . Drastic changes in the frequency of ν_1 were observed between each phase. ν_1 gradually shifted to higher wavenumbers upon heating until the VII/III transition was reached, at which point it decreased abruptly before increasing further to the III/II change. At the III/II transition, ν_1 again decreased and continued to decrease through the II/I transition; it then increased steadily to the melting point. The halfwidth of ν_2 showed discontinuous increases at each of the transitions, but the halfwidth of ν_1 showed little or no abrupt changes as it increased steadily to the melting point.

There is some dispute as to whether or not KNO_2 III is fully ordered. Solbakk and Stromme (1969)⁸ studied the x-ray pattern of a single crystal and suggested no rotational disorder was present; Richter and Pistorius (1972)⁷ used crystallographic and thermodynamic measurements but were unable to present conclusive results; and Adams et al (1988)⁴⁰ concluded the Raman spectra of KNO_2 III indicated the existence of some disorder. The 252 K spectrum presented in figure 27 is very much like that recorded by Adams et al (1988)⁴⁰ at 253 K. It shows *two* broad lattice modes extending from the Rayleigh wing and a very weak ν_3 mode which merges into the ν_1 mode. As Adams et al (1988)⁴⁰ concluded, it does resemble more closely the spectrum of the disordered phase, KNO_2 II. KNO_2 III does appear to be disordered but the presence of two lattice bands means it is not fully disordered. These results are also consistent with the calorimetric study of Mraw et al (1978)¹⁴. Although Mraw et al (1978) did not observe the VII/III transition, they noted the order-disorder transition actually began at about 90 K. In fact, the low frequency Raman modes show increasing character of disorder with increasing temperature (figure 28). Despite the fact KNO_2 III appears to contain some disorder, the greatest disorder of the nitrite ions seems to occur at the III/II transition. It is at this transition that the greatest structural changes in the internal modes are noted.

The room temperature spectrum of KNO_2 II is consistent with that of a disor-

dered solid (figure 29). It displays a featureless Rayleigh wing and displays ν_3 as a low-frequency shoulder of ν_1 . ν_3 is even more smeared out in the high-temperature spectrum of KNO_2 I which is very similar to the room-temperature spectrum. The structural changes in ν_1 and ν_2 at the II/I phase transition therefore are very discrete as seen in figure 27. This is not surprising since the nitrite ions are going from an already orientationally disordered state, Rln12, to a more orientationally disordered state, Rln32. Tse et al (1986)⁴³ conclude there are no abrupt spectral changes in the three internal modes between 300 and 430 K indicating the phase transition of KNO_2 from phase I to phase II does not change the basic crystal symmetry. However, they report spectral evidence of a phase transition around 380 K. In the present study there were no sudden changes in the peak positions or halfwidths of ν_1 or ν_2 between 320 K and the melting point, hence there is no evidence for a phase change in this region. More specifically, there is no indication of the phase transition observed at about 380 K in the Raman study by Tse et al (1986)⁴³, nor of the 363 K transition suggested by Tanisaki and Ishimatsu (1965)⁴².

The spectral changes in ν_1 and ν_2 at the melting point are consistent with those of Pnyazhnyi et al (1976)²¹. The frequency of ν_1 increases upon heating and at the melting point shifts abruptly to a higher wavenumber. The frequency of ν_2 , on the other hand, remains constant above room temperature until the melting point where it decreases sharply.

Comparison of the high-temperature spectrum (figure 30) with the melt spectra (figures 31,32) show they are very much alike. The low-frequency: ν_2 mode: ν_1 mode integrated peak intensity ratio for the melt is 1:9:12 and that for the melt is 1:8:12.

Hirotsu et al (1981)² determined the molar entropy of fusion for KNO_2 to be $10.5 \text{ JK}^{-1}\text{mol}^{-1}$ which is only slightly greater than the molar entropy for the II/I transition, $7.01 \text{ JK}^{-1}\text{mol}^{-1}$ (Mraw et al, 1978)¹⁴. The value of $10.5 \text{ JK}^{-1}\text{mol}^{-1}$ for fusion of KNO_2 is typical for that of a plastic crystal⁶⁸. The molar entropy of the

III/II, order-disorder transition however is much greater than these, $23.54 \text{ JK}^{-1}\text{mol}^{-1}$. This is completely in agreement with the spectral results obtained in this study as it further demonstrates that the majority of the disorder occurs at the III/II transition at about 260 K. It would be very interesting to obtain a value of the energy for the VII/III phase transition. Spectroscopic measurements appear to indicate that the value would be about the same as that for the II/I transition.

RbNO₂

The polymorphism in rubidium nitrite has been studied by several workers and the crystal structure of at least two polymorphs of the salt have been determined. Natarajan and Hovi (1972)⁴⁴ reported a phase transition at 360 K based on dta and electrical conductivity measurements, while Natarajan and Rao (1975)¹⁵ also used DTA to obtain a transition temperature of 340 K with a molar enthalpy change of $2100 \text{ J}\cdot\text{mol}^{-1}$. Similar measurements by Protsenko and Kolmin (1971)⁴⁵ gave a transition at about 261 K. Calorimetric investigations by Richter and Pistorius (1972)¹⁰ and Boak and Staveley (1987)¹⁵ also produced a transition around this temperature, 264.2 K and 263.7 K respectively. Molar enthalpies and entropies determined for this transition are reported in Table 2. In addition to the above transition, Boak and Staveley (1987)¹⁵ observed two minor anomalies, one between 225-248.6 K and the other 400-45 K, with molar enthalpy changes of $71 \text{ J}\cdot\text{mol}^{-1}$ and $310 \text{ J}\cdot\text{mol}^{-1}$ respectively. Hirotsu et al (1981)² observed a transition at a slightly lower temperature, 252 K, using elastic softening measurements.

The low-temperature structure, RbNO₂ II is monoclinic, proposed space group C_{2h}^3 ($B_{2/m}$ or $C_{2/m}$) (Hirotsu et al, 1981)² with $a_0 = 8.904$, $b_0 = 4.828$, $c_0 = 8.185 \text{ \AA}$ and $\beta = 115.9^\circ$; whereas, the high-temperature structure, RbNO₂ I is face-centered cubic, space group O_h^5 (F_{m3m}) with $a_0 = 6.934 \text{ \AA}$.

The phase transition in RbNO₂ has not been previously studied by vibrational

spectroscopy; the only reported spectrum being a Raman spectrum of the melt by Prisyazhnyi et al (1976).²¹

Spectra obtained at various temperatures for a pure and an impure rubidium nitrite sample are illustrated in figures 34 to 41. Table 9 gives the peak frequencies of the Raman spectra for the solid phases and the melt, and Table 10 gives the frequencies and halfwidths for the ν_1 and ν_2 modes at all temperatures used over the range investigated.

At 84 K, (figure 34) the lattice and internal modes are very sharp and well defined indicating RbNO₂ II is an ordered solid. The room-temperature spectrum (figure 35) however is clearly that of a disordered solid; the lattice modes are a part of the broad Rayleigh wing and ν_3 is smeared out as a shoulder on the low-frequency side of a much broader ν_1 band. Therefore the transition from phase II to phase I for RbNO₂ must be an order-disorder transition with respect to the orientations of the nitrite ions, a result consistent with the elastic softening experiments of Hirotsu et al (1981).²

The progress of the nitrite ion disordering is presented in figure 36. Discontinuities in the ν_1 and ν_2 frequencies and halfwidths were present between 209 K and 235 K and between 256 and 298 K (figure 42). The most marked change was in the position of the ν_2 peak which shifted from 812.5 cm⁻¹ at the phase transition. The appearance of the 802.5 cm⁻¹ band became evident at 209 K, and at 235 K a complete shift from 812.5 cm⁻¹ to 802.5 cm⁻¹ occurred.

In addition, the phase change was monitored by "sitting" on the ν_2 peak at 812.5 cm⁻¹ while slowly warming and cooling over the transition temperature. Sudden changes in the intensity were recorded and the phase transition was estimated to occur at 225 K (figure 43).

As indicated earlier, recent experiments have indicated the phase transition occurs closer to 260 K; there is evidence for this transition in figure 42. The lower

Figure 34. Raman spectrum of RbNO_2 II recorded at 84 K using the blue 4880 Å line. $\nu_{\text{initial}} = 30 \text{ cm}^{-1}$. This is the low temperature ordered phase.

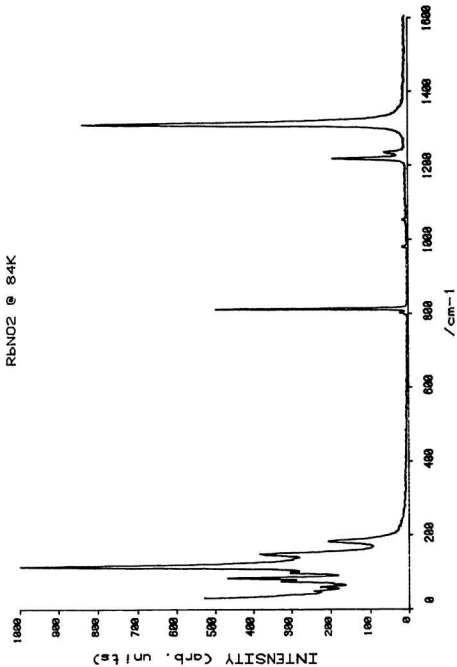


Figure 35. Raman spectrum of RbNO_2 I recorded at 298 K using the blue 4880 Å line. $\nu_{\text{initial}} = 30 \text{ cm}^{-1}$. This is the disordered phase.

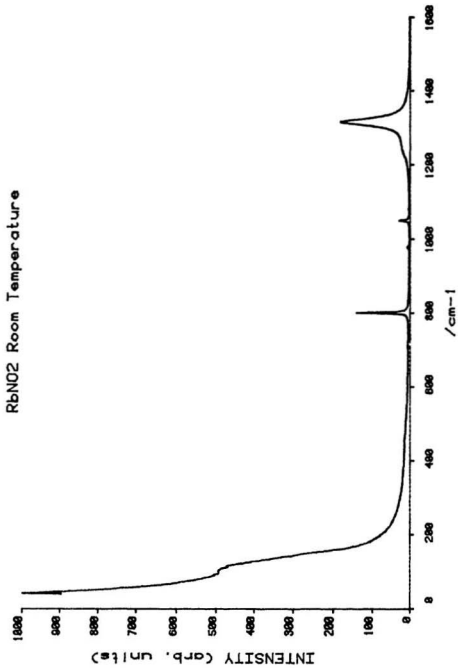


Figure 36. Raman spectra of RbNO_2 as it went through the order-disorder phase transition (~ 224 K). The spectra were recorded using the blue 4880 \AA line at: A) 84 K; B) 184 K; C) 209 K; and D) 235 K. $\nu_{\text{initial}} = 30 \text{ cm}^{-1}$.

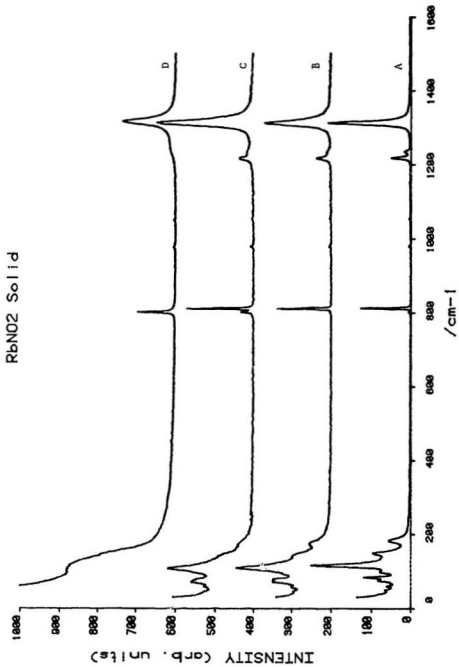


Figure 37. Raman spectrum of NO_3^- impure RbNO_2 recorded at 91 K using the blue 4880 Å line. $\nu_{\text{initial}} = 20 \text{ cm}^{-1}$. The nitrite occupies two sites as seen by the doublet at 802.5 and 814.0 cm^{-1} . Not completely ordered.

RbNO₂ Impure @ 91K

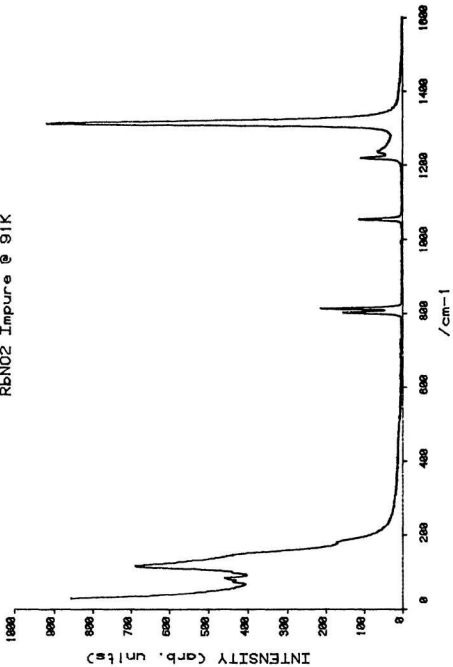


Figure 38. Raman spectra of NO_3^- impure RbNO_2 as it went through the order-disorder phase transition. Spectra were recorded using the blue 4880 \AA line at: A) 91 K; B) 166 K; C) 216 K; and D) 241 K. $\nu_{\text{initial}} = 30 \text{ cm}^{-1}$.

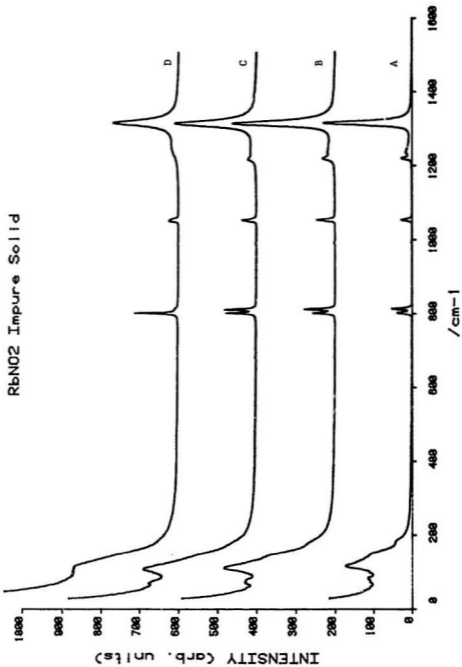


Figure 30. Raman spectrum of RbNO_2 recorded at 670 K using the blue 4880 Å line.

$\nu_{\text{initial}} = 50 \text{ cm}^{-1}$. This is the disordered room temperature phase.

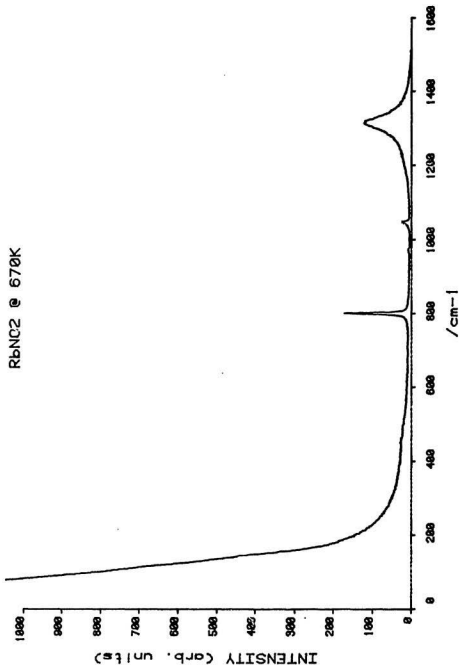


Figure 40. Intensity, $I(\omega)$, Raman spectra of RbNO_2 melt recorded at 703 K using the green 5145 Å line. $\nu_{\text{initial}} = 54 \text{ cm}^{-1}$.

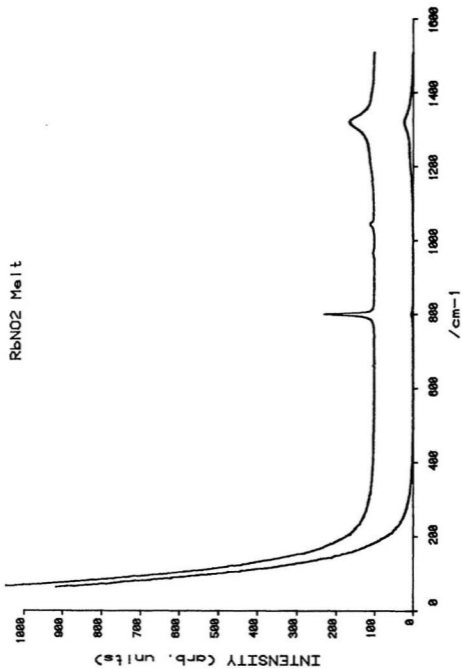


Figure 41. Reduced, $R(\omega)$, Raman spectra of RbNO_2 melt recorded at 703 K using the green 5145 Å line. $\nu_{\text{initial}} = 54 \text{ cm}^{-1}$.

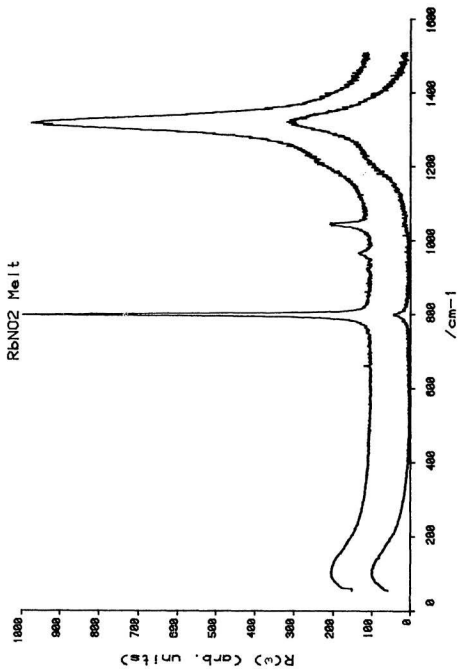


Table 9. Peak Frequencies (in cm^{-1}) for the Different Phases of Rubidium Nitrite.

84 K II	234 K ?	298 K I	670 K I	703 K I	Assignment
49.0 (m,sp)					ν_L
59.5 (m,sp)					ν_L
68.5 (sh)					ν_L
75.5 (s,sp)					ν_L
84.0 (s,sp)					ν_L
99.0 (sh)					ν_L
	~ 120			102.0 (w,br)	ν_L
115.5 (vs,sp)					ν_L
130.0 (sh)					ν_L
149.5 (s,sp)					ν_L
183.0 (m,sp)					ν_L
802.5 (vw)	802.5	801.5 (s,sp)	801.0 (s,sp)	800.5 (m,sp)	ν_2
812.5 (s,sp)					ν_2
980 (vw)		980 (vw)	980 (vw)	980 (vw)	$\nu_1(\text{SO}_4^{2-})$
1054 (vw)		1054 (w)	1054 (w)	1054 (w)	$\nu_1(\text{NO}_3^-)$
1218.5 (m,sp)		1240 (sh)	-	-	ν_3
1313.0 (vs,sp)		1316.5 (s,sp)	1314.0 (m,br)	1320.5 (m,br)	ν_1

Table 10. Peak Frequencies and Halfwidths of ν_1 and ν_2 for Rubidium Nitrite at Various Temperatures.

Temperature/K	ν_1 frequency (halfwidth)/cm ⁻¹	ν_2 frequency (halfwidth)/cm ⁻¹
84	1313.0 (10.8)	812.5 (3.4)
109	1313.0 (10.8)	812.5 (3.4)
135	1313.0 (13.6)	812.5 (3.4)
159	1313.5 (15.0)	812.0 (3.4)
184	1314.0 (17.0)	811.5 (3.4)
209	1314.5 (20.3)	811.5 (3.4)
234	1318.0 (23.8)	802.5 (5.4)
253	1317.0 (23.7)	802.5 (5.4)
298	1316.5 (25.0)	801.0 (4.7)
670	1314.0 (51.9)	801.0 (5.4)
703	1320.5 (55.4)	800.0 (6.9)

Figure 42. Temperature dependence of ν_1 and ν_2 frequency and halfwidth for RbNO_2 .

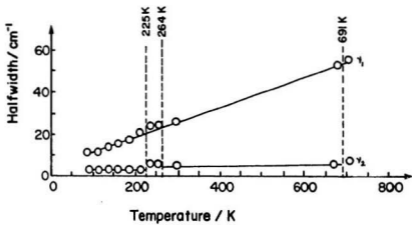
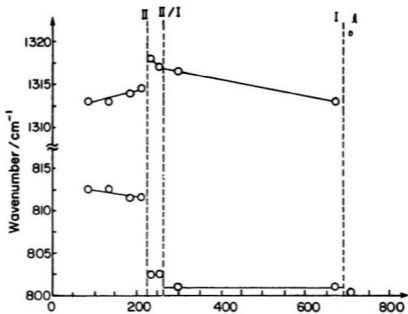
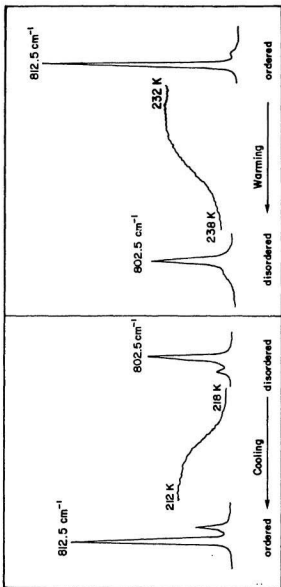


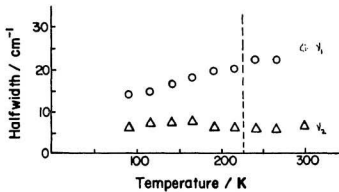
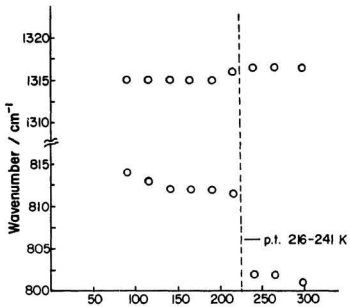
Figure 43. RbNO₂ peak being monitored through phase transition.



phase transition in this study at about 225 K may be: (1) due to nitrate impurity, a nitrate impurity is known to cause the phase transitions in KNO_2 to be sluggish (Bridgman, 1915⁶⁹; and Rapoport 1966⁷⁰); (2) the result of an order-disorder phase transition; or (3) due to the formation of a nitrite/nitrate solid solution complex.

Inspection of the spectrum recorded at 84 K shows the presence of a very weak peak due to the NO_3^- symmetric stretch at about 1050 cm^{-1} (figure 34). In addition, there is a very weak peak at 802.5 cm^{-1} , indicating the presence of some disorder in the ordered solid. Addition of nitrate impurity appears to increase the disorder in RbNO_2 II as evidenced by the spectrum of NO_3^- impure RbNO_2 at 91 K (figure 37). This spectrum is comparable to the spectrum of the more pure sample recorded at 209 K (figure 36); both spectra exhibit considerable broadening of the lattice modes and both contain a ν_2 doublet with comparable peaks present at 802.5 cm^{-1} and 812.5 cm^{-1} . Note the intensity of the low frequency nitrite peak is enhanced due to added NO_3^- (figure 37) but the peak is due to a form of nitrite not nitrate because NO_3^- does not have a Raman active mode at this frequency. The progress of the phase transition in nitrate impure RbNO_2 is presented in figure 38 and the behaviour of ν_1 and ν_2 frequencies and halfwidths is shown in figure 44. Once again, the RbNO_2 is completely disordered before the reported phase transition of 260 K. The frequency of ν_1 showed a discontinuous change between 191 and 216 K while the ν_2 frequency showed a marked change between 216 and 241 K. No discontinuities were noted in the halfwidths of ν_1 or ν_2 . While it appears the presence of nitrate impurity may indeed render the transition in RbNO_2 sluggish, and it may even prevent orientational ordering of the nitrite ions at low temperatures, it does not appear to influence the transition at 225 K. If it had, the addition of nitrate would enhance this transition. This effect was not observed. Also, the amount of NO_3^- impurity present in the "pure" sample is extremely small, therefore the formation of a nitrite/nitrate complex is unlikely. This leaves the possibility for an order-disorder

Figure 44. Temperature dependence of ν_1 and ν_2 frequency and halfwidth for impure RbNO_2 .



transition at about 225 K. The lattice mode and $\nu_1 - \nu_3$ peaks in the spectrum for the sample at 235 K are consistent with a disordered solid; the spectrum illustrates a featureless Rayleigh wing and ν_3 is a broad shoulder of ν_1 . Therefore, a new, disordered phase of RbNO_2 may exist between 225 K and 260 K. This transition supports the anomaly observed between 225 and 248.6 K by Boak and Staveley (1987)¹⁵.

The low-temperature spectrum of RbNO_2 II has ten observable peaks due to external vibrations plus the three internal mode peaks characteristic to the nitrite ion. Factor group analysis predicts 12 normal modes of vibration, all Raman active, assuming RbNO_2 II has space group C_{2h}^3 with four molecules per unit cell. ($5A_g + 7B_g$ or $6A_g + 6B_g$ or $7A_g + 5B_g$ for Rb and N with C_2 , C_s or C_i site symmetries respectively.) Therefore, it appears RbNO_2 II belongs to a higher symmetry space group than predicted by Hirotsu et al (1981)².

As RbNO_2 I was heated, there were no sudden changes recorded in the frequencies or halfwidths of ν_1 and ν_2 before melting. The high-temperature spectrum is presented in figure 39. However characteristic changes were observed upon melting (figure 42). The ν_1 frequency decreased steadily to the melting point where it increased greatly; Prisyazhnyi²¹, on the other hand observed an increase in ν_1 frequency on heating. The behaviour of ν_2 however was consistent with Prisyazhnyi; ν_2 decreased very slightly on heating and decreased a further 1 cm^{-1} upon melting. The halfwidths of these peaks also showed sudden increases at the solid-liquid transition.

The discontinuities are not as great for the solid-liquid transition as for the order-disorder change which is to be expected since most of the orientational disorder of the NO_2^- ions has already occurred at the II/I transition. In fact, comparison of the entropies of each transition shows that the entropy of the order-disorder transition is $32.3 \text{ J}\cdot\text{K}^{-1}\cdot\text{mol}^{-1}$ whereas it is only $9.40 \text{ J}\cdot\text{K}^{-1}\cdot\text{mol}^{-1}$ for the melting of RbNO_2 .² This low entropy associated with melting is characteristic of that for

plastic crystals.⁶⁸

The spectra of molten RbNO_2 are illustrated in figures 40 and 41. The similarity with the high-temperature spectrum, once again stresses the orientational disorder of the NO_2^- ions present in RbNO_2 I.

CsNO_2

There are many discrepancies in the reported polymorphism of cesium nitrite. Protsenko and Kolomin (1971)⁴⁵ reported phase transitions at 175 K and 353 K; Natarajan and Hovi (1972)⁴⁴ discovered a 365 K phase transition based on dta and conductivity measurements; Natarajan and Rao (1975)¹⁵ reported a transition at 303 ± 10 K; Richter and Pistorius (1972)¹⁰ determined a transition at 179 K using dta; Mraw and Staveley (1976)¹⁷ recorded a 208.85 K transition based on a calorimetric investigation, and Moriya et al (1983, 1981)¹⁶ also used calorimetric data to determine a transition of 209.16 K.

The room-temperature crystal structure of CsNO_2 I is of the CsCl type, space group O_h^1 (P_{m3m}) with one molecule per unit cell and the nitrite ions orientationally disordered (Pistorius and Richter, 1972)¹⁰. It transforms at about 209 K to a rhombohedral structure, II, of space group D_{3d}^3 (R_{3m}) where the orientational disorder of the nitrite ions is believed to persist (Moriya et al, 1983, 1981)¹⁶. Calorimetric studies conducted by Mraw and Staveley (1976)¹⁷ and by Moriya et al (1983, 1981)¹⁶ showed no evidence for reported transitions at 353 K, 365 K or 393 K, however Mraw and Staveley did observe a minor anomaly at 408 K. Moriya also observed a glass transition at 42 K which they believed is freezing of the ionic disorder in CsNO_2 . Thus, the possibility of a third, ordered phase of CsNO_2 solid at regular pressure exists.

Cesium nitrite has been the subject of very few vibrational spectroscopic investigations. Moriya et al¹⁶, in addition to their calorimetric investigations, studied the

ν_2 region of the Raman spectrum for the II/I transition; Carr et al (1979)¹⁹ recorded a Raman spectrum at 18 K; Brooker and Irish (1971)²⁰ obtained Raman and infrared spectra at room-temperature; and Prisyazhnyi et al (1976)²¹ studied CsNO_2 melt using Raman spectroscopy. A detailed study covering all the phases of CsNO_2 has not been done before this investigation.

Raman spectra obtained for cesium nitrite over the temperature range 84 K to the melting point, 679 K, and for the melt are illustrated in figures 45 to 51. Only one solid-solid phase transition was recorded in this investigation, the II/I transition. Table 11 gives peak frequencies for the solid phases and the melt, and Table 12 gives the ν_1 and ν_2 frequencies and halfwidths at all the temperatures used over the range studied.

The low-temperature spectrum of CsNO_2 II (figure 45) is consistent with an ordered crystal; the internal modes are sharp and well defined as are the lattice modes. This spectrum resembles that recorded by Carr et al (1979)¹⁹ at 18 K, and does not support the thesis held by Moriya et al (1983, 1981)¹⁶ of a low-temperature disordered phase. Further, if there is a phase transition at about 42 K as proposed by Moriya et al (1983, 1981)¹⁶, the Raman spectra at 18 K and 84 K indicate the basic crystal symmetry of CsNO_2 II does not change.

The room-temperature spectrum of CsNO_2 I is clearly that of a disordered solid (figure 46); the internal modes are much broader and ν_3 appears as a shoulder on ν_1 while the low-frequency region displays a featureless Rayleigh wing. Raman spectra were recorded over the transition temperature and spectral changes noted (figures 47,52). There was a slight discontinuous decrease in the frequency of ν_1 at the transition which occurred between 183 K and 208 K, but no discontinuity in the ν_1 halfwidth which increased upon heating was detected. The greatest change occurred in the ν_2 mode. At 184 K it appeared as a sharp peak at 806 cm^{-1} but became an unresolved doublet centered around 801.5 cm^{-1} upon transition to the disordered

Figure 45. Raman spectrum of CsNO₂ II recorded at 83 K using the blue 4880 Å line. $\nu_{\text{initial}} = 20 \text{ cm}^{-1}$. This is the low temperature ordered phase.

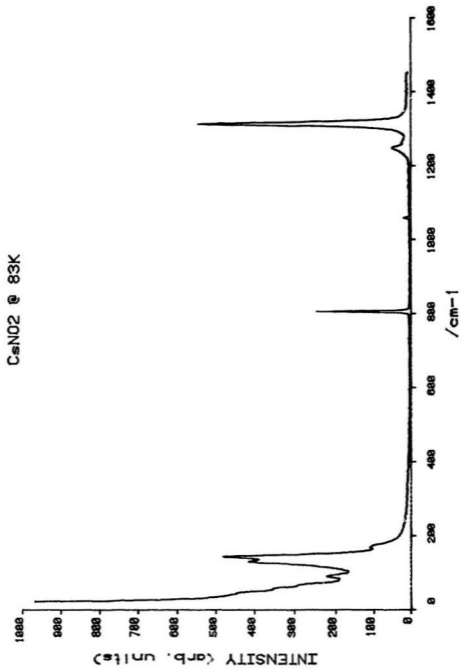


Figure 46. Raman spectrum of CsNO_2 I recorded at 298 K using the blue 4880 Å line. This is the disordered phase.

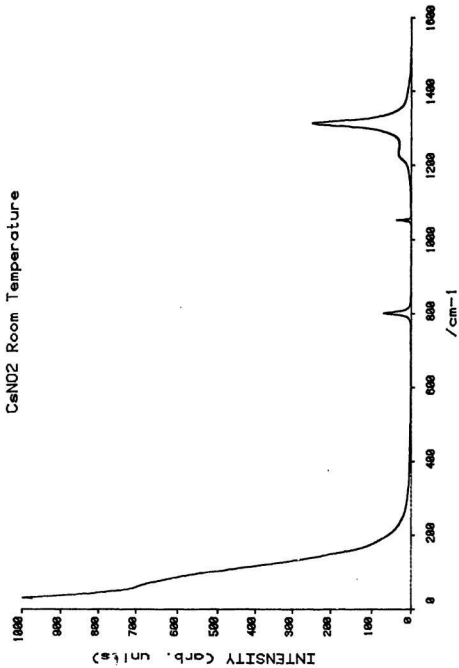


Figure 47. Raman spectra of CsNO_2 as it went through the order-disorder phase transition (~ 163 K). Spectra were recorded using the blue 4880 \AA line at: A) 83 K; B) 183 K; C) 208 K; and D) 233 K. $\nu_{\text{initial}} = 20 \text{ cm}^{-1}$.

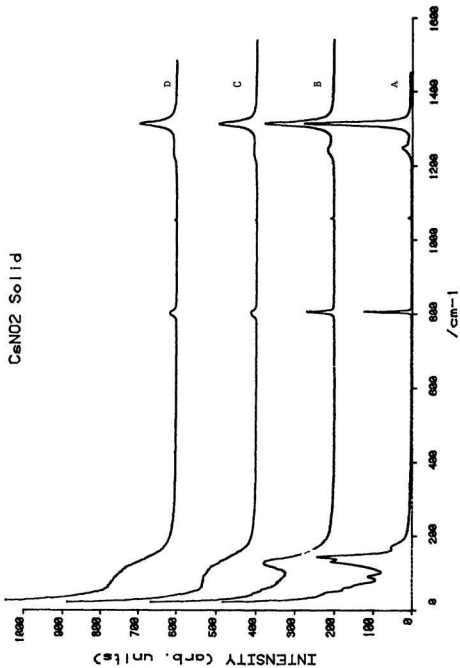


Figure 48. Raman spectra of the ν_2 mode as it went through the order-disorder phase transition at about 193 K. Conditions as specified in Figure 47 except for the temperatures A) 83 K, B) 183 K, C) 208 K, and D) 233 K ν_2 for RbNO_2 at 183 K and 208 K was curve resolved into two Lorentzian components.

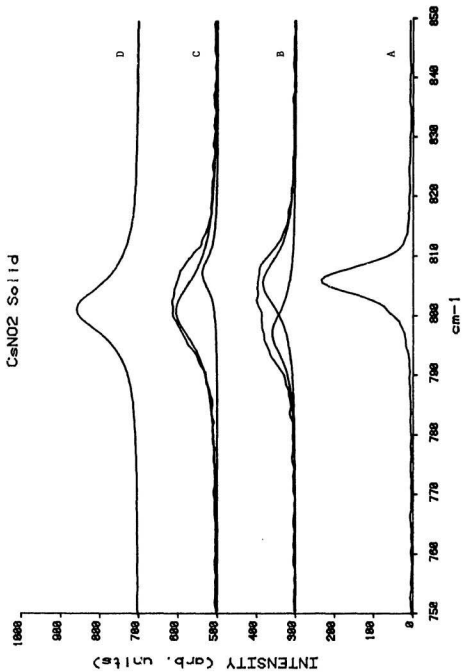


Figure 49. Raman spectrum of CsNO₂ I recorded at 650 K using the blue 4880 Å line. The spectrum is that of the disordered room temperature phase.

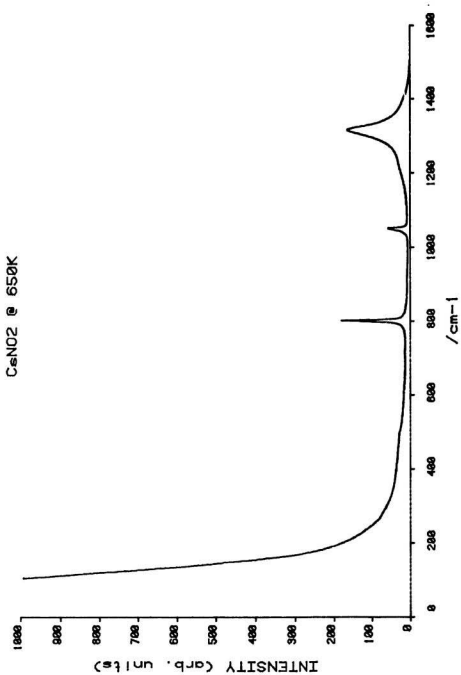


Figure 50. Intensity, $I(\omega)$, Raman spectra of CsNO_2 melt recorded at 783 K using the blue 4880 Å line. $\nu_{\text{initial}} = 40 \text{ cm}^{-1}$.

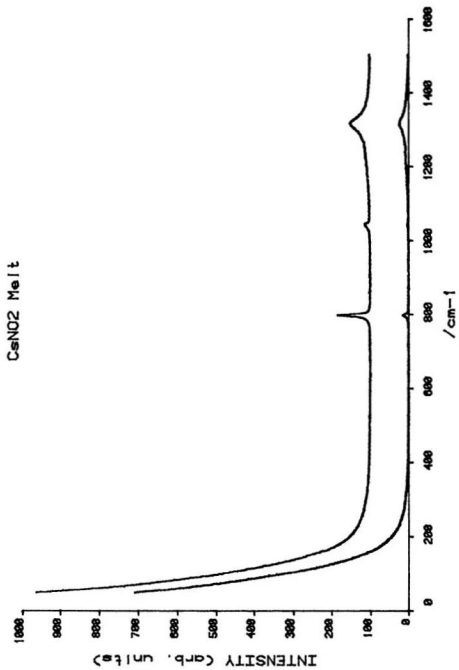


Figure 51. Reduced, $R(\omega)$, Raman spectra of CsNO_2 melt recorded at 783 K using the blue 4880 Å line. $\nu_{\text{initial}} = 40 \text{ cm}^{-1}$.

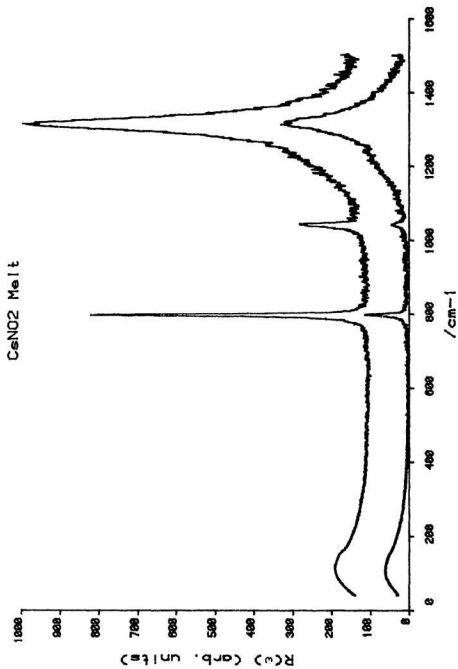


Table 11. Peak Frequencies (in cm^{-1}) for the Different Phases of Cesium Nitrite.

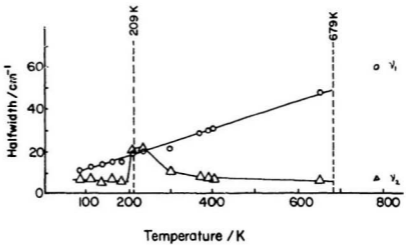
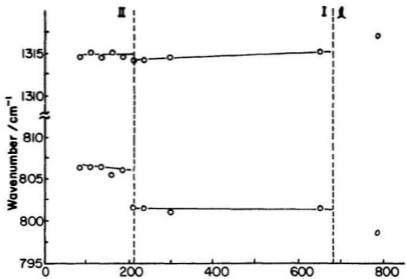
83 K II	298 K I	650 K I	783 K I	Assignment
48 (sh)				ν_L
56 (sh)				ν_L
68 (sh)				ν_L
90.5 (m,sp)			102 (w,br)	ν_L
130.0 (s,sp)				ν_L
143.5 (s,sp)				ν_L
168. (sh)				ν_L
806.5 (s,sp)	801.0 (m,sp)	801.5 (m,sp)	798.5 (in,sp)	ν_2
1060 (vw)	1052 (w)	1052 (w)		$\nu_1(\text{NO}_2^-)$
1249.0 (w,sp)	1228 (w,br)	-	-	ν_3
1314.5 (s,sp)	1314.5 (s,sp)	1315.0 (br)	1317.0 (br)	ν_1

Table 12. Peak Frequencies and Halfwidths of ν_1 and ν_2 for Cesium Nitrite* at Various Temperatures.

Temperature/K	ν_1 frequency (halfwidth)/cm ⁻¹	ν_2 frequency (halfwidth)/cm ⁻¹
83	1314.5 (11.0)	806.5 (6.9)
108	1315.0 (12.3)	806.5 (6.9)
133	1314.5 (14.0)	806.5 (5.5)
158	1315.0 (15.0)	805.5 (6.9)
183	1314.5 (15.0)	806.0 (5.5)
208	1314.0 (19.0)	801.5 (20.7)*
233	1314.0 (20.0)	801.5 (20.7)*
298	1314.5 (21.0)	801.0 (10.4)
367	1314.5 (28.4)	801.5 (8.0)
387	1314.5 (29.6)	801.5 (7.6)
397	1314.5 (30.0)	801.5 (6.4)
650	1315.0 (47.6)	801.5 (6.8)
783	1317.0 (59.8)	798.5 (7.6)

* Unresolved doublet.

Figure 52. Temperature dependence of ν_1 and ν_2 frequency and halfwidth for CsNO_2 .



phase. Once again, presence of some nitrate impurity appears to have lowered the transition temperature from 209 K slightly. In fact, this may also explain the lower transition temperature of 179 K reported by Richter and Pistorius (1972)¹⁰ since they thought their sample was nitrate impure. The same may also be true for the reported transition at 175 K (Protsenko and Kolomin, 1971).⁴⁵

The ν_2 doublet at 208 K and 233 K was resolved into two Lorentzian components as illustrated in figure 48. This splitting arises from existence of two non-equivalent crystallographic sites for NO_2^- in the cubic lattice of CsNO_2 I (Moriya et al, 1983).¹⁶

Based on packing and symmetry considerations the nitrite ion can be oriented such that the O-O axis is parallel to the body-diagonal axis, as it occurs in the low temperature structure, or parallel to the face diagonal axis of the cubic structure. The internal vibrations of the NO_2^- ions in the two non-equivalent crystallographic orientations are influenced by different crystal fields thus they have different frequencies. The frequency of the bending mode in the low-temperature, ordered phase is close to that of the high-frequency component of the doublet above the transition, whereas the low-frequency component of the doublet is close to the frequency of the bending mode at room-temperature. Therefore the high-frequency component is due to the NO_2^- ion oriented with its O-O axis parallel to the body-diagonal axis. Moriya et al (1983)¹⁶ have labelled the low-frequency component as such, but there is no immediate explanation for this. As the temperature increases, reorientational motion increases rapidly and an average of the two different orientations is observed by vibrational spectroscopy measurements. The result is motional narrowing which leads to a broad singlet peak as recorded in the room temperature spectrum.

No further discontinuities were noted in either ν_1 or ν_2 before melting of the solid. In particular, no evidence was found for transitions around 353 K, 365 K, or 393 K; nor was any evidence found for an anomaly at 408 K.

The frequency of ν_2 remained constant on heating to the melting point whereas the frequency of ν_1 increased slightly. When the sample was melted, ν_1 increased sharply while ν_2 decreased, which is consistent with the observation of Prisyazhnyi et al (1976)²¹. Only slight changes in halfwidths of these peaks were detected at the melting point, and in fact the high temperature spectrum at 650 K (figure 49) looks like the spectra of the melt (figure 50,51). This again demonstrates that much of the orientational disorder of the nitrite ion has occurred at the order-disorder phase change. Thermodynamic data is also in complete agreement with this observation, the entropy of transition for the II/I transition, $17.2 \text{ JK}^{-1}\text{mol}^{-1}$, is greater than that for the melting, $13.7 \text{ JK}^{-1}\text{mol}^{-1}$.

Anomalous Bands

There were several anomalous bands observed in the spectra of the solid alkali metal nitrites. The low temperature Raman spectra of ordered lithium, potassium, rubidium and cesium nitrite solids all showed a band between the ν_1 and ν_3 modes (1305, 1275, 1232 and 1263 cm^{-1} respectively). In addition spectra of NaNO_2 single crystals exhibited bands at about 1189 cm^{-1} and 1490 cm^{-1} . Possible assignments for these anomalous bands include the following:

- (1) Correlation field components of the ν_3 mode.
- (2) ν_3 (LO) peaks observed at intermediate positions for the unoriented samples.
- (3) Isotopic NO_2^- modes due to ^{15}N or ^{18}O . However the shifts do not match those reported for $^{15}\text{NO}_2^-$ and $\text{N}^{16}\text{O}^{18}\text{O}^-$ by Kato and Rolfe⁷¹.
- (4) Impurity effects such as that observed in the ν_2 region of impure RbNO_2 . Impurities could give rise to pockets of solid solution with Raman active modes that are superimposed on the spectrum of the ordered solid.
- (5) Combination and difference bands with external modes^{72,73}.

Molten Salts

The fact that the Raman spectra of the molten and high temperature nitrites resemble those of aqueous nitrites suggests the spectra may be interpreted on the basis of the free-ion approximation modified by nearest neighbour interactions. Furthermore the peak maxima for the I_{iso} and I_{aniso} components in the molten salts are identical to within one wavenumber which suggests the absence of intermolecular coupling between neighbouring nitrite pairs.

For example consider the spectroscopic measurements of aqueous KNO_2 ; Table 13 gives the peak positions and halfwidths for 2.0 M and 14.0 M KNO_2 aqueous solutions. When the halfwidth of the anisotropic spectrum (Γ_{aniso}) is greater than that of the isotropic spectrum (Γ_{iso}) the difference can be ascribed to reorientational relaxation. The values of Γ_{R} are 14 cm^{-1} and 7 cm^{-1} for the ν_1 and ν_2 modes of 2.0 M KNO_2 respectively whereas $\Gamma_{\text{R}} = 0 \text{ cm}^{-1}$ for these modes in the 14 M solution. The fact that $\Gamma_{\text{iso}} = \Gamma_{\text{aniso}}$ for the latter solution suggests the reorientational motion is totally hindered due to increased interactions (hydrogen bonding) between NO_2^- and H_2O . The increased viscosity of the concentrated solution reflects the same effect.

The spectroscopic measurements of the molten alkali metal nitrite salts are presented in Table 14. Two trends should be noted for the ν_1 and ν_2 modes: first the halfwidth of the isotropic component (Γ_{iso}) which is only due to vibrational relaxation and is considered to come from elastic or inelastic collisions with other molecules decreases Li to Cs; second Γ_{R} due to reorientational relaxation also tends to increase Li to Cs although there is considerable uncertainty for the CsNO_2 value. Since the halfwidths of the polarized components are mainly affected by vibrational dephasing, the broadening can be interpreted in terms of the distribution of vibrational energy states due to elastic NO_2^- - cation interactions and the difference in the range of environments. (See figure 53 for an example). Lithium has the greatest homogeneous broadening or greatest range of environments since it has greatest Γ_{iso}

Table 13. Peak Frequencies and Halfwidths for Aqueous KNO_2 .

2.0 M			14.0 M			
Frequency cm^{-1}	Γ_{aniso} cm^{-1}	Γ_{iso} cm^{-1}	Frequency cm^{-1}	Γ_{aniso} cm^{-1}	Γ_{iso} cm^{-1}	Assignments
-	-	-	87	100	-	NO_2^- reorientation
180	100	-	170	102	-	H_2O hydrogen bond
815	24	17 ^a	806	18	18	ν_2
1050			1050			$\nu_1(\text{NO}_3^-)$
1232	67	-	1235	67	-	ν_3
1328	54	40 ^b	1332	40	40	ν_1

a. $\Gamma_{\text{R}} = 7 \text{ cm}^{-1}$

b. $\Gamma_{\text{R}} = 14 \text{ cm}^{-1}$

Γ_{R} = the halfwidth of the band due to reorientational relaxation. $\Gamma_{\text{R}} = \Gamma_{\text{aniso}} - \Gamma_{\text{iso}}$.

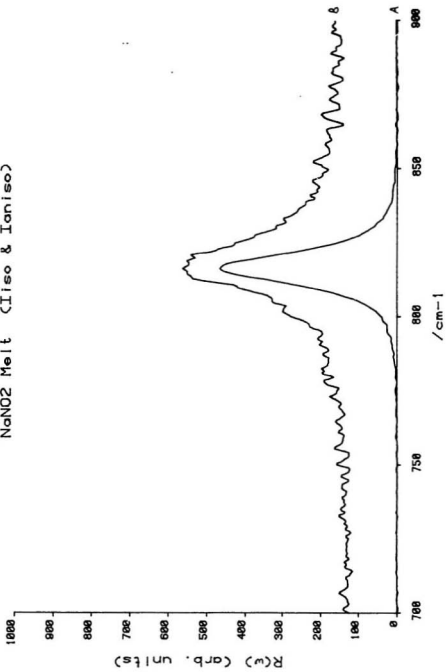
Table 14. Peak Frequencies and Halfwidths for Molten Alkali Metal Nitrites.

LiNO ₂	NaNO ₂	KNO ₂	RbNO ₂	CsNO ₂	Assignments
153	112	105	102	102	reorientation
~300	~250	sh	sh	sh	
840 (43,45) ^a	816 (13,21)	803 (8.7,24)	800 (7.1,18)	798 (6.2,18 ^b)	ν_2
1060	1055	1050	1050	1050	$\nu_1(\text{NO}_3^-)$
1246 (100)	1232 (97)	1220 (103)	1215 (105)	1210 (105)	ν_3
1354 (67,82)	1338 (57,75)	1323 (43,94)	1319 (40,88)	1313 (30,88 ^b)	ν_1

- a. The halfwidths for the isotropic ($\Gamma_{\text{iso}} = \Gamma_{\text{V}}$) and the anisotropic ($\Gamma_{\text{aniso}} = \Gamma_{\perp}$) spectra are given in parentheses. $\Gamma_{\text{R}} = \Gamma_{\perp} - \Gamma_{\text{V}}$
- b. Halfwidths estimated after correction for spill-over of isotropic component.

Figure 53. Reduced, $R(\omega)$, Raman spectra of NaNO_2 melt recorded at 573 K using the green 5154 Å line. $\nu_{\text{initial}} = 44 \text{ cm}^{-1}$. (A) $I_{\text{iso}} = I_{||} - 1.3I_{\perp}$. (B) $I_{\text{aniso}} = I_{\perp}$

NaNO₂ Melt (Iiso & Ianiso)



(Γ_{vib}). Increased cation size leads to less cation mobility, for example Cs^+ has more inertia and therefore the cation structure about the nitrite has a longer lifetime and a smaller range of environments. Fewer orientations exist and a narrower density of states is observed. Thus, an increase in cation mass is reflected in smaller values of Γ_{vib} .

On the other hand, rotational freedom is more favoured by the larger cation K^+ , Rb^+ and Cs^+ nitrites which have much larger values of Γ_{R} . The considerably smaller Γ_{R} values for LiNO_2 are consistent with a decrease in the rotational mobility of NO_2^- perhaps due to specific pair interactions. These conclusions are also consistent with the fact that the peak maximum of the low frequency mode shifts with cation, and also reflects the effect of collisions, or time between collisions, between the anions and cations. The maximum of the low frequency mode for molten LiNO_2 (153 cm^{-1}) is much higher than that for either of the K, Rb, or Cs salts indicating that reorientation is less favoured for LiNO_2 melt. It is also interesting to note that the values of Γ_{R} from the ν_1 data are approximately the same for the K, Rb and Cs nitrite melts ($\sim 50 \text{ cm}^{-1}$) as are the peak maximum of the low frequency mode for each melt ($\sim 102 \text{ cm}^{-1}$).

The low frequency intensity has been shown to be depolarized and it exhibits distinct band structure in the high temperature solids and melts when plotted in the $R(\omega)$ format. Depolarized intensity in the low frequency region of disordered solids and liquids of anisotropic molecules and ions has been attributed to reorientation motions of the polarizability anisotropy. The fact that the feature is present in aqueous solution suggests that the intensity is a monomolecular property and is not due to collective properties. Similar results have been reported for many liquids and solutions.^{56,57,66,74}

It is interesting that there are two low frequency features present in the lithium and sodium melts. As with the Na solid the mode at smaller wavenumber is due to

restricted rotation about the molecular b axis whereas the higher wavenumber band is the result of restricted rotation of the NO_2^- ion about the molecular c axis. The fact that the nitrite ion has pseudo symmetric top symmetry and may be considered as a disc of similar shape to the nitrate ion would suggest that reorientation about the a axis (top axis) should not have a large associated polarizability change.

The relative intensities of the Raman modes are essentially constant over the solid phases, aqueous solutions and melts for all of the alkali metal nitrites (Table 15). The relative intensity of the low frequency mode is approximately proportional to the polarizability anisotropy squared (β^2). Table 16 shows a comparison of the measured and calculated β^2 ratio values for nitrite in addition to other oxyanions. The measured and experimental values are in close agreement.

In addition, results have indicated that the depolarization ratios for the molten salts and aqueous solutions are essentially independent of cation. Although experimental difficulties caused primarily by sample decomposition (bubbles) resulted in appreciable errors for the lithium and cesium melts, the sodium, potassium, rubidium and aqueous solutions gave results that were consistent within a 10% error.

Table 15. Alkali Metal Nitrite Melts. Depolarization Ratios and Integrated Intensity Ratios.

Mode	ρ	Intensity Ratio
low frequency	0.75	0.19
ν_2	0.11	0.11
ν_3	0.75	0.15
ν_1	0.30	1.0

Table 16. Polarizability Anisotropies for Nitrites and Other Oxyanion Systems.

Anion	β^2	β^2 Ratio	Measured intensity ratio
NO_3^-	3.84	100	100
NO_2^-	4.72	123	150
CO_3^{2-}	1.12	29	22
ClO_3^-	0.55	14	14
ClO_4^-	0	0	1

LEAF 161 OMITTED IN PAGE
NUMBERING.

FEUILLET 161 NON INCLUS DANS
LA PAGINATION.

National Library of Canada,
Canadian Theses Service.

Bibliothèque nationale du Canada,
Service des thèses canadiennes.

CONCLUSION

The spectra of the alkali metal nitrites have been obtained. Many of the spectra, particularly for LiNO_2 , RbNO_2 and CsNO_2 have been reported for the first time. This spectroscopic method has proven to be quite useful in following the phase transitions in these salts. Also, the details of an ab initio study of these salts has been reported. The spectroscopic and theoretical calculations have proven especially useful in studying the order-disorder phase transition for NaNO_2 . Raman spectra of molten nitrites were measured and interpreted to indicate faster reorientation relaxation and slower vibrational relaxation with increased cation size.

REFERENCES

1. Hathaway, B.J and Slade, R.C., *J. Chem. Soc. A*, *1485* (1966).
2. Hirotsu, S., Miyamoto, M., and Yamamoto, I., *Japanese Journal of Applied Physics*, *20*(12), *L917-919* (1981).
- 3a. Irish, D.E., "In Ionic Interactions, Dilute Solutions to Molten Salts." Vol. 2, S. Petrucci. (Editor) Academic Press, New York. 1971. Chap. 9. p. 187.
- 3b. Durand, D., Dénoyer, F., Currat, R., and Lambert, M., in "Incommensurate Phases in Dielectrics", Vol. 2, Blinc, R., and Levanyuk, A.P. (Editors) Elsevier, Holland, 1986, p. 101.
- 3c. Brooker, M.H., and Irish, D.E., *Can. J. Chem.*, *46*, *229* (1968).
4. Wyckoff, R.W.G., "Crystal Structures" (Wiley, New York, 1964), 2nd ed., Vol. 2, Chap. VII A.
5. Zeigler, G.E., *Phys. Rev.*, *38*, *1040* (1931).
- 6a. Tanisaki, S., *J. Phys. Soc. Japan*, *16*, *579* (1961).
- 6b. Strijk, B., and MacGillavry, C.H., *Rec. Trav. Chim.*, *62*, *705* (1943); *65*, *127* (1946).
7. Pistorius, C.W.F.T., and Richter, P.W., *Z. anorg. allg. Chem.*, *389*, *315-320* (1972).
8. Solbakk, J.K., and Stromme, K.O., *Acta Chem. Scand.*, *23*(1), *300-313* (1969).
9. Ray, J.D., *J. Inorg. Nucl. Chem.*, *15*, *269* (1960).
10. Richter, P.W., and Pistorius, C.W.F.T., *J. Sol. State Chem.*, *5*(2), *276-285* (1972).
11. Stern, K.H., *J. Phys. Chem. Ref. Data*, *1*(3) (1972).
12. *Nouveau Traité de Chimie Minérale*, Paul Pascal, Editor, Masson et C^{ie}, Paris, 1957.

- 13a. Nomura, S., *J. Phys. Soc. Japan*, **16**, 1352 (1961).
- 13b. Hartwig, C.M., Wiener-Avnear, E., and S.P.S. Porto, *Phys. Rev.*, **B5**, 79 (1972).
14. Mraw, S.C., Boak, R.J., and Staveley, L.A.K., *J. Chem. Thermodynamics*, **10**, 359-368 (1978).
15. Boak, R.J., and Staveley, L.A.K., *J. Chem. Thermodynamics*, **19**, 661-670 (1987). And unpublished reference therein; Natarajan, M., and Rao, C.N.R. (1975).
16. Moriya, K., Matsu, T., and Suga, H., *J. Phys. Chem. Solids*, **44**(12) 1103-1119, 1121-1132 (1983); *Chem. Phys. Lett.*, **82**(3), 581-585 (1981).
17. Mraw, S.C., and Staveley, L.A.K., *J. Chem. Thermodynamics*, **8**, 1001-1007 (1976).
18. Hermansson, K., and Thomas, J.O., *Acta Cryst.*, **C39**, 930-936 (1983).
19. Carr, R., Vanos, J., and Torrie, B.H., *Chem. Phys. Lett.*, **65**(1), 73-76 (1979).
20. Brooker, M.H., and Irish, D.E. *Can. J. of Chem.*, **49**, 1289-1295 (1971).
21. Prisyazhnyi, V.D., Kirillov, S.A., and Snezhkov, V.I., Translated from *Zhurnal Prikladnoi Spektroskopii*, **25**(6), 1058-1061, (1976).
22. Sawada, S., Nomura, S., Fujii, S., and Yoshida, I., *Phys. Rev. Lett.*, **1**, 320 (1958).
23. Brehat, F., and Wyncke, B., *J. Phys. C.: Solid State Phys.*, **18**, 1705-1720 (1985).
24. Jurneau, D., *Phys. Stat. Solidi. (b)*, **106**, 149 (1981).
25. Goncharuk, I.N., and Chisler, E.V., *Soviet. Phys. Solid State*, **18**(2) (1976).
26. Ivanova, E.A., and Chisler, E.V., *Soviet. Phys. Solid State*, **17**(10) (1976).
27. Chisler, E.V., and Shur, M.S., *Phys. State. Solidi.*, **17**, 173 (1966).
28. Sato, Y., Gesi, K., Takagi, Y., *J. Phys. Soc. Japan*, **16**(11) (1961).

29. Iio, K., and Yanagi, T., *J. Phys. Soc. Japan*, *35*(5), 1465-1471 (1973).
30. Vogt, H., and Happ, H., *Phys. Status Solidi*, *B44*, 207 (1971).
31. Ota, K., Ishibashi, Y., and Takagi, Y., *J. Phys. Soc. Japan*, *29*(6) (1970).
32. Ehrhardt, E.D., and Michel, K.H., *Z. Physik B: Condensed Matter*, *41*, 329-339 (1981); *Phys. Rev. Lett.*, *46*(4) (1981).
33. Lynden-Bell, R.M., Impey, R.W., and Klein, M.L., *Chem. Phys.*, *109*, 25-33 (1986).
34. Klein, M.L., and MacDonald, I.R., *Proc. R. Soc. Lond.*, *A382*, 471-482 (1982).
35. Kay, M.I., Gonzalo, J.A., Maglic, R., *Ferroelectrics*, Vol. *9*, 179-186 (1975).
36. Niumura, N., and Muto, M., *J. Phys. Soc. Japan*, *35*, 628 (1973).
37. Shibuya, I, et al, *J. Phys. Soc. Japan*, *28*, Supplement (1970).
38. Suzuki, S., Murakami, H., and Takagi, M., *J. Phys. Soc. Japan*, *50*(2), 555-562 (1981); also Suzuki, S., and Takagi, M., *J. Phys. Soc. Japan*, *39*(1) (1971).
39. Betsuyaku, H., *J. Phys. Soc. Japan*, *27*(6) (1969).
40. Adams, D.M., Pogson, M., and Sharma, S.K., *J. Phys. C: Solid State Phys.*, *21*, 623-637 (1988).
41. Adams, D.M., and Sharma, S.K., *Solid State Communications*, *23* 729-731 (1977); *ibid*, *Chem. Phys. Lett.*, *39*(3), 407-409 (1975).
42. Taniski, S., and Ishimatsu, T., *J. Phys. Soc. Japan*, *20*, 1277 (1965).
43. Tse, W.S., Pai, K.F., and Lih, W., *Annual Report of the Institute of Physics, Academia Sinica*, *16*, 223-8 (1986).
44. Natarajan, M., Hovi, V., *Annls. Acad. Sci. Fenni. Serv. VI Phys.*, No. 400 (1972).
45. Protsenko, P.I., Kolomin, L.G., *Izv. Vyssh. Ucheb. Zaved. Fiz.*, *14*, 105 (1971), (*Chem. Abstr.* 1971, 75, 123665b).

46. Brooker, M.H., "The Chemical Physics of Solvation, Part B", Dogonadze, R.R., et. al., (Editors) Chapter 4, p. 119, Elsevier, Amsterdam, 1988.
47. Long, D.A., "Raman Spectroscopy", McGraw-Hill, New York, 1977.
48. Cotton, F.A., "Chemical Applications of Group Theory", Interscience, New York, 1963.
49. Ross, S.D., "Inorganic Infrared and Raman Spectra", McGraw-Hill, London, 1972.
50. Placzek, G., "Rayleigh-Streuung und Raman-Effekt", ed. E. Marx, Handbuch der Radiologie, Vol. 6, Part 2, 2nd ed., Akademische Verlag, Leipzig, 1934, p. 205.
51. Gordon, R.G. in "Advances in Magnetic Resonance", Vol. 3, John Waugh (Editor), Academic Press, 1968. For a good example see Kato, T., and Takenaka, T., Mol. Phys., 43, 1083 (1981).
52. Bhagavantam, S., and Venkatarayudu, T., "Theory of Groups and Applications to Physical Problems", Andhra University Press, Waltair, India, 1951.
53. Fateley, W.G., et al, "Infrared and Raman Selection Rules for Molecular and Lattice Vibrations: The Correlation Method", Wiley Interscience, USA, 1972.
54. Halford, R.S., J. Chem. Phys., 14, 8 (1946).
55. Damen, T.C., Porto, S.P.S., and Tell, B., Phys. Rev., 142, 570 (1966).
56. Perrot, M., Brooker, M.H., and Lascombe, J., J. Chem. Phys., 74, 2787 (1981).
57. Lund, P.A., Faurskov Nielson, O. and Praestgaard, Chem. Phys., 28, 167 (1978); J. Chem. Phys., 75, 1586 (1981).
58. Wolkenstein, M., Compt. Rend. Acad. Sci. U.R.S.S., 32, 185 (1941).
59. Protsenko, P.I., and Bordyushkova, Russian Journal of Inorganic Chemistry, 10 (5), 657, (1965).

60. Barnes, J.C., and Sesay, L.J., *J. Less Common Metals*, **63**, 301 (1979).
61. Gafurov, M.M., *Sov. Phys. Solid State*, **26**(4), 719-720 (1984).
62. Andrade, P. da R., et al, *Solid State Communications*, **12**, 847-851 (1973).
63. Gesi, K.J., *J. Phys. Soc. Japan*, **26**, 953 (1969).
64. Von der Lieth, C.W., and Eysel, H.H., *Journal of Raman Spectroscopy*, **13**, 2 (1982).
65. Iqbal, Z., and Owens, F.J., "Vibrational Spectroscopy of Phase Transitions", Academic Press Inc., USA, 1984.
66. Baroski, M.K., and Ballantyne, J.M., *Phys. Rev.*, **174**(3), 946-952 (1968).
67. Parry, G.S., Schuyff, A., and Ubbelohde, A.R., *Proc. Roy. Soc. A*, **285**, 360-369 (1964).
68. Sherwood, J.N., "The Plastically Crystalline State", Sherwood, J.N. (Editor), John Wiley and Sons, New York, 1979, p. 39.
69. Bridgman, P.W., *Proc. Amer. Acad. Arts Sci.* **72**, 45 (1937).
70. Rapoport, E., *J. Chem. Phys.*, **45**, 2721 (1966).
71. Kato, R. and Rolfe, J., *J. Chem. Phys.* **47**, 1901 (1967).
72. Chisler, E.V., Davydov, V. Yu., Goncharuk, I.N., Ivanova, E.A., *Phys. Stat. Solidi*, **679**, 347 (1977).
73. Holah, G.O., *J. Phys. C: Solid State Physics*, **4**, 2191 (1971).
74. Brooker, M.H., and Papatheodorou, G.N., in "Advances in Molten Salt Chemistry", Amsterdam 1983.

APPENDIX 1

Abstract

The optimum geometries for the nitro and nitrito forms of Li, Na, K and Rb nitrite free molecules, as obtained from ab initio calculations, are reported; nitrito is the more stable form. STO-3G and 3-21G basis sets were used. Energies for transition between the nitro and nitrito structures of NaNO_2 were calculated (with the addition of 6-31G* basis set). The in-plane rotation about the a axis occurs in two steps with a new minimum energy intermediate. Finally, the polarizabilities of nitrito NaNO_2 were calculated using 6-31G** basis set and compared with experiment. These results are consistent with various experimental measurements which indicate the order-disorder phase transition in NaNO_2 favours an in-plane NO_2 rotation about the a axis.

This paper first deals with optimized geometries for the nitro and nitrito forms of free Li, Na, K and RbNO_2 molecules. Second, the polarizability of nitrito NaNO_2 along the a, b, and c axes is presented. Then, rotations of the NO_2 group about the a and c axes for nitrito NaNO_2 (leading to nitrito to nitro transition) are considered. Energy potentials for the transitions are calculated. Possible implications of these transitions and the polarizability for free NaNO_2 on the order-disorder phase transition of the crystal are discussed.

Method

All calculations were done ab initio using the MONSTERGAUSS series of computer programs.¹ Optimized geometries for the nitro and nitrito forms of Li, Na, K, and Rb nitrite were obtained using the OC method of Davidson.² Minimal STO-3G basis set was first used and optimized geometries obtained by such were then used as initial guesses for geometries obtained using 3-21G basis set.³ The second form of the nitrito structure, which contains two alkali metal ions per NO₂ group, required open shell SCF calculations. These were attempted using restricted Hartree-Fock (RHF) and unrestricted Hartree-Fock (UHF) approaches.

The electronic polarizability of the nitrito form of NaNO₂ was calculated by electric field scanning using an applied field of 0.0005 au and 0.0015 au for 6-31G* basis set.³ The following conversion factors were used in the calculations:

$$1 \text{ Debye} = 3.33564 \times 10^{-30} \text{ C}\cdot\text{m}^4$$

$$1 \text{ au of electric field} = 5.1422506 \times 10^9 \text{ V/cm}$$

$$1 \text{ \AA}^3 = 1.112607 \times 10^{-40} \text{ C}^2\cdot\text{m}^2\cdot\text{J}^{-1} \text{ (22)}$$

The transition between nitrito NaNO₂ and nitro NaNO₂ was studied using single point calculations for STO-3G basis set.³ First the Na-N-O angle was varied such that an in-plane rotation of the NO₂ group about the crystallographic a axis was obtained. The energy, obtained from the single point calculations, for various angles was plotted against the angle of rotation. Two additional structures of interest were thus discovered, a minimum energy and a saddle point structure. Optimized geometries, using STO-3G, 3-21G and 6-31G*³ basis sets were calculated for the four structures of NaNO₂. Note, the optimized geometry for the saddle point, energy maximum, structure was obtained using an adaptation of the VA05 method described by Powell.⁵ Similarly, single point calculations for an out-of-plane rotation about the c axis to achieve a nitrito transition were done.

Results

(I) Optimized geometries

A C_{2v} symmetry restriction was imposed when optimizing the geometries for both the nitro and nitrito nitrite structures. The results for the nitro structures are presented in Table A1 and those for the nitrito structures are in Table A2.

An experimentally determined geometry for NaNO_2 has been determined by Kay and Fraser.⁶ This experimental geometry of NaNO_2 crystal compares favorably with the theoretically determined geometry of a free nitrito NaNO_2 molecule using 6-31G* basis set.

	NaNO_2 experimental ⁶	OC, 6-31G*
Na-O	$2.471 \pm 0.004 \text{ \AA}$	2.19526 \AA
Na-N	2.589 ± 0.009	2.589470
N-O	1.240 ± 0.003	1.230432
$\angle \text{ONO}$	$114.9 \pm 0.5^\circ$	115.5050°

The calculated Na-O atomic distance is slightly smaller than the experimental value, however the other values are in excellent agreement. The 6-31G* basis set greatly improved the STO-3G and 3-21G basis sets calculations for NaNO_2 . The present calculations indicate that the nitrito form is more stable for the alkali metal nitrites. Relative energies of the nitro and nitrito forms are presented in Table A3. In all cases except LiNO_2 , STO-3G, the nitrito forms are more stable, that is lower in energy. The exception for LiNO_2 may be due to the fact that LiNO_2 has been reported to exist in both forms, coupled with the fact of course that STO-3G basis set is not as accurate as 3-21G.

The X-N, X-O atomic distances increase from Li to Rb for both the nitro and nitrito nitrites. However, the N-O distances and O-N-O angles vary in no apparent

Table A1: Nitro geometries

STO-3G					
X→	Li	Na	K	Rb	
X-N /Å	1.773240	2.056228	2.531764	2.651046	
N-O /Å	1.281181	1.286262	1.284097	1.286999	
<ONO/	120.9086	118.2962	118.4118	117.4320	
3-21G					
X-N /Å	1.349799	2.136802	2.533729	2.634019	
N-O /Å	1.261908	1.265885	1.271142	1.269676	
<ONO/	121.9196	121.1460	120.2200	120.9464	

Table A2(a): Nitrito geometries

STO-3G					
X→	Li	Na	K	Rb	
X-N /Å	1.865144	2.409328	2.893645	3.030559	
X-O /Å	1.91715	1.98346	2.44484	2.55746	
N-O /Å	1.368312	1.296349	1.286943	1.290653	
<ONO/	141.6716	110.7080	114.0780	113.1440	
3-21G					
X-N /Å	2.226887	2.559409	2.993155	3.106100	
X-O /Å	1.84084	2.14271	2.54170	2.64697	
N-O /Å	1.294043	1.288198	1.285422	1.285975	
<ONO/	111.4666	113.4306	114.7068	114.9524	

Table A2(b):

	STO-3G		3-21G	
X→	Li	Na	Li	Na
N-O /Å	1.372263	1.432041	1.407396	1.405054
X-O /Å	1.619439	1.876436	1.682125	1.997041
<ONX/	113.2536	119.8764	115.5746	113.9150
<XON/	74.2279	80.6197	77.5812	82.3280

Table A3: Energies/ Hartrees, nitro and nitrito
STO-3G

X--	Li	Na	K	Rb
Nitro	-208.626952	-361.185482	-794.388773	-3108.99471
Nitrito	-208.529978	-361.272017	-794.477250	-3109.06205
3-21G				
Nitro	-210.308734	-363.762578	-799.060072	-3127.64010
Nitrito	-210.384545	-363.823389	-799.105408	-3127.69183

set pattern. This unusual trend is very puzzling.

Studies of the open shell nitrito structures are incomplete at this point. Results have been obtained for Li and Na using the RHF approach. (Table A2(b)). However, due to problems in dealing with large atoms such as K and Rb, the RHF calculations have not yet been completed. Also, it was found that for this series of molecules, at the low basis sets used calculations by the UHF approach were not valid due to spin contamination. This problem could possibly be rectified by using higher basis sets. It should be noted that this open shell structure may play an important role in the order-disorder phase transition mechanism.

(II) Electronic Polarizability

The electronic polarizability for the nitrito form of NaNO_2 calculated along the a, b and c axes are reported in Table A4.

Table A4

	6-31G*, F = 0.001 au	Experiment ¹
$\alpha_{xx}(\alpha_{cc})$	3.56	4.610
$\alpha_{yy}(\alpha_{aa})$	1.68	2.240
$\alpha_{zz}(\alpha_{bb})$	2.65	2.716
$\bar{\alpha}$	2.63	3.19
μ	7.827740 Debyes	-
β	1.66	2.17
β^2	2.75	4.72

Net atomic charges are N = +0.43071, Na = +0.74099 and each O = -0.58585.

Once again, the theoretical calculations performed here agree reasonable well with the experimental calculations. The values may be improved by carrying out a

differential method theoretical calculation. In any respect, the present calculations explicitly show that the polarizability lies mostly in the bc plane - that is in the plane of the molecule. Since the polarizability is proportional to the number of electrons, most of the electrons lie in the molecular bc plane. Therefore, based on this study an out-of-plane rotation would be less favored since it will require a much greater polarizability change.

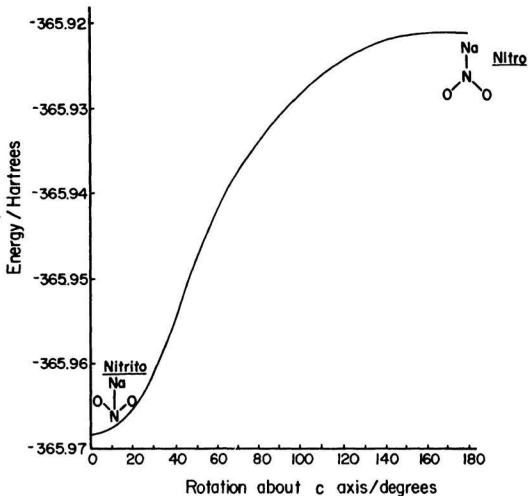
This calculation also demonstrates the validity of comparing calculations performed on a free NaNO_2 molecule with the solid crystal.

(III) Transition in NaNO_2

A nitrito to nitro transition can be obtained by a 180° rotation of the NO_2 group about either the a or c axis. Rotation of the NO_2 group for NaNO_2 (nitrito) about either the a or c axis will lead to the nitro structure. However, in a series of molecules which exist in the solid state, the same molecular structure results, except the dipole moment of the NO_2 group points in the opposite direction, and the NO_2 group interacts with the Na atom of a neighbouring molecule. The out-of-plane rotation about the c axis is a direct transition, that is, there are no intermediate maximum or minimum points. The energy barrier is simply the energy difference between the nitrito and nitro forms, 0.047219 Hartrees. The relationship between energy and angle of rotation can be seen in Graph A1. Similar results were obtained using 3-21G basis sets. However the STO-3G basis set, unlike 3-21G + 6-31G*, indicates the nitro form is a stable one. Results of the in-plane rotation proved to be very interesting. The relationship between this rotation and energy can be seen in Graph A2. From this study it can be seen that the Na atom has two equilibrium positions (that is energy minimums) about the NO_2 group and two maxima energy positions, the nitro being the highest energy structure. The optimized geometries for these structures are given in Table A5. The unidentate structure (an energy maximum) is a saddle point. Similar results were obtained for STO-3G and 3-21G basis

Graph A1

Energy potential for nitro transition
via out-of-plane rotation about c-axis.



Graph A2

Energy potential for nitrito to nitro transition via an in-plane rotation about a-axis

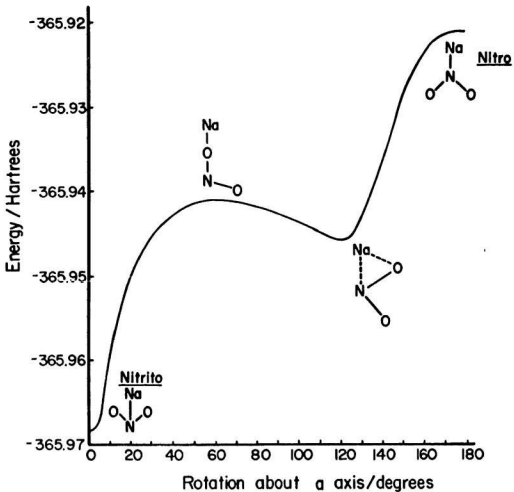
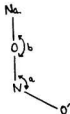


Table A5:

Nitro Transition min Saddle point Nitrito



STO-3G

E=	-361.185482	-361.226778	-361.203537	-361.272017 Hart
Na-N=	2.056228	2.206804	3.15276	2.409328 A
N-O =	1.286262	1.345830	1.324116	1.296349 A
N-O' =	--	1.253284	1.257954	-- A
Na-O=	--	1.90657	1.83073	1.98346 A
a =	118.2862	114.7122	112.4769	110.7080
b =	--	59.1471	184.2205	--

3-21G

E=	-363.762578	-363.796332	-363.794969	-363.823389 Har
Na-N=	2.136802	2.246234	3.24472	2.559409 A
N-O =	1.265885	1.338872	1.327986	1.288198 A
N-O' =	--	1.219282	1.224719	-- A
Na-O=	--	2.04203	1.917003	2.14271 A
a =	121.1460	118.0252	114.4984	113.4306
b =	--	63.6653	178.5043	--

6-31G*

E=	-365.921144	-365.945701	-365.941031	-365.968363 Har
Na-N=	2.204461	2.280873	3.23202	2.589470 A
N-O =	1.214178	1.259490	1.269749	1.230432 A
N-O' =	--	1.186259	1.185633	-- A
Na-O=	--	2.11187	1.976696	2.19526 A
a =	120.8010	118.3355	115.3488	115.5050
b =	--	66.0893	191.0742	--

sets as seen in Table A5.

The question arises, which transition is favored, the 180° rotation about the a axis or the 180° rotation about the c axis?

The less hindered out-of-plane rotation about the c axis may be expected to be more favored. However, this is not the case as the present study shows. The out-of-plane rotation has a calculated energy barrier of 0.047219 Hartrees (Graph A1). The in-plane rotation, on the other hand, appears to be facilitated by a 'transition minimum' structure indicated in Graph A2. The energy barrier to this structure is 0.024557 Hartrees, and the barrier between this intermediate structure and the resulting nitro structure is 0.027332 Hartrees. This 'two-step' transition appears to be consistent with the experimentally observed order-disorder transition for $\text{NaNO}_2(\text{s})$. As the temperature (energy) is increased, the 'transition minimum' becomes populated, (thus forming the incommensurate phase). Further increase in temperature results in a transition between the "transition minimum" and the nitro structure, since this only requires 0.027332 Hartrees compared with 0.047219 Hartrees for the out-of-plane rotation.

If the order-disorder transition is realized by such a rotation, it is conceivable that the antiferroelectric phase which is stable between the ordered and disordered phases (163-164°C), may have a structure containing molecules with a geometry similar to the 'transition minimum' molecule. The net result is that the transition for free NaNO_2 favors a 'two-step' in-plane 180° rotation about the a axis.

Conclusion

The theoretical results obtained in this work for a free NaNO_2 molecule indicate the order-disorder phase transition in the crystal is most probably realized by a 180° rotation of the NO_2 group about the crystallographic a axis.

The results do not agree with molecular dynamics calculations of Lynden-Bell⁸,

et al., and Ehrhardt and Michel⁹. However, the molecular dynamics calculations assume point charges whereas this study takes into consideration the electronic charge distribution and gives a more accurate account of the interactions since the transition does involve a polarizability change. Also, as this study found, the bonding between Na and NO_2^- does contain considerable covalent character.

It would be interesting to continue these calculations for order-disorder phase transitions observed in other molecules such as KNO_2 and RbNO_2 .

The results are also consistent with the fact that the alkali metal prefers to attach to NO_2 through the oxygens (nitrito).

At present, work is under way by this author studying the LO mode of a single crystal of NaNO_2 through the phase transition by Raman spectroscopy.

References

1. M.R. Peterson and R.A. Poirier, MONSTERGAUSS, Dept. of Chem., Univ. of Toronto, Toronto, Canada and Dept. of Chem., Memorial Univ. of Newfoundland, St. John's, Can.
2. W.C. Davidson and L. Nazareth, Technical Memos 303 and 306, 1977, Applied Mathematics Division Argonne National Laboratories, Argonne, Illinois. The Algorithm is described in W.C. Davidson, *Math. Prog.* **9**, 1 (1975).
3. R.A. Poirier, R.E. Kari and I.G. Csizmadia, *Handbook of Gaussian basis sets* (Elsevier, Amsterdam, 1985).
4. P.W. Atkins, *Physical Chemistry*, W.H. Freeman and Company, San Francisco, USA, 1978.
5. M.J.D. Powell, *Numerical Methods of Nonlinear Algebraic Equations*, P. Rabinowitz (Ed.), Gordon and Breach, London (1970), p. 87.
6. M.I. Kay and B.C. Fraser, *Acta Cryst* **14**, 56 (1961).
7. S. Hirotsu, et al., *J. Phys. Soc. Jpn.*, **25**, 799 (1968).
8. R.M. Lynden-Bell, et al., *Chem. Phys.* **109**, 25-33 (1986).
9. K.D. Ehrhardt and K.H. Michel, *Phys. Rev. Lett.* **46**, 291-294 (1981) and *Z. Phys. B* **41**, 329 (1981).

